



Nanoscopic Analysis Reveals an Orderly Arrangement of the Presynaptic Scaffold Protein Bassoon at the Golgi-Apparatus

Tina Ghelani^{††}, Carolina Montenegro-Venegas^{2,3,4}, Anna Fejtova^{2,5,6} and Thomas Dresbach^{1*}

¹ Institute of Anatomy and Embryology, University Medical Center Göttingen, Göttingen, Germany, ² Department of Neurochemistry and Molecular Biology, Leibniz Institute for Neurobiology, Magdeburg, Germany, ³ Center for Behavioral Brain Sciences, Magdeburg, Germany, ⁴ Institute for Pharmacology and Toxicology, Medical Faculty, Otto von Guericke University, Magdeburg, Germany, ⁵ Department of Psychiatry and Psychotherapy, University Hospital Erlangen, Friedrich-Alexander Universität Erlangen-Nürnberg, Erlangen, Germany, ⁶ RG Presynaptic Plasticity, Leibniz Institute for Neurobiology, Magdeburg, Germany

OPEN ACCESS

Edited by:

Arnaldo Parra-Damas,
Universitat Autònoma de Barcelona,
Spain

Reviewed by:

Elisa D'Este,
Max Planck Institute for Medical
Research (MPIMF), Germany
Andreas Martin Grabrucker,
University of Limerick, Ireland

*Correspondence:

Thomas Dresbach
thomas.dresbach@med.uni-
goettingen.de

† Present address:

Tina Ghelani,
Molecular and Theoretical
Neuroscience,
Leibniz-Forschungsinstitut für
Molekulare Pharmakologie, FMP im
CharitéCrossOver (CCO) Charité -
University Medicine Berlin, Berlin,
Germany

Specialty section:

This article was submitted to
Neuroplasticity and Development,
a section of the journal
Frontiers in Molecular Neuroscience

Received: 19 July 2021

Accepted: 22 September 2021

Published: 05 November 2021

Citation:

Ghelani T,
Montenegro-Venegas C, Fejtova A
and Dresbach T (2021) Nanoscopic
Analysis Reveals an Orderly
Arrangement of the Presynaptic
Scaffold Protein Bassoon
at the Golgi-Apparatus.
Front. Mol. Neurosci. 14:744034.
doi: 10.3389/fnmol.2021.744034

Bassoon is a core scaffold protein of the presynaptic active zone. In brain synapses, the C-terminus of Bassoon is oriented toward the plasma membrane and its N-terminus is oriented toward synaptic vesicles. At the Golgi-apparatus, Bassoon is thought to assemble active zone precursor structures, but whether it is arranged in an orderly fashion is unknown. Understanding the topology of this large scaffold protein is important for models of active zone biogenesis. Using stimulated emission depletion nanoscopy in cultured hippocampal neurons, we found that an N-terminal intramolecular tag of recombinant Bassoon, but not C-terminal tag, colocalized with markers of the *trans*-Golgi network (TGN). The N-terminus of Bassoon was located between 48 and 69 nm away from TGN38, while its C-terminus was located between 100 and 115 nm away from TGN38. Sequences within the first 95 amino acids of Bassoon were required for this arrangement. Our results indicate that, at the Golgi-apparatus, Bassoon is oriented with its N-terminus toward and its C-terminus away from the *trans* Golgi network membrane. Moreover, they suggest that Bassoon is an extended molecule at the *trans* Golgi network with the distance between amino acids 97 and 3,938, estimated to be between 46 and 52 nm. Our data are consistent with a model, in which the N-terminus of Bassoon binds to the membranes of the *trans*-Golgi network, while the C-terminus associates with active zone components, thus reflecting the topographic arrangement characteristic of synapses also at the Golgi-apparatus.

Keywords: Golgi, STED, Bassoon, synapse assembly, synaptogenesis

INTRODUCTION

Scaffold proteins recruit and anchor molecules to subcellular sites. Due to their multi-domain and modular structure, they bind and regulate multiple proteins to coordinate biochemical reactions in space and time. Employing scaffold proteins is a fundamental principle of cell function, operating during protein folding, receptor and signaling molecule clustering, and at cell-cell junctions (Good et al., 2011).

Synapses are asymmetric cell-cell junctions assembled and regulated by scaffold molecules. On the presynaptic side, a set of synaptic scaffold proteins confines the docking of synaptic vesicles and

the exocytotic release of a neurotransmitter from these vesicles to specialized sites of the axonal plasma membrane, called active zones. Several families of scaffold proteins operate at active zones, including RIMs, RIM-binding proteins, Munc13s, α -liprins, and ELKS/CAST/ERC proteins, as well as the particularly large scaffold proteins Bassoon and Piccolo (Südhof, 2012; Gundelfinger et al., 2016). One way by which the presynaptic machinery acts is through RIMs, which recruit both voltage-gated calcium channels and Munc13s, a family of proteins essential for making synaptic vesicles tethered at the active zone fusion competent (Südhof, 2012; Imig et al., 2014; Acuna et al., 2016). Bassoon regulates this core transmitter release machinery, at least at some synapses, by selectively recruiting the P/Q type of voltage-gated calcium channels and by speeding up synaptic vesicle reloading to release sites during ongoing activity (Hallermann et al., 2010; Davydova et al., 2014; Mendoza Schulz et al., 2014). In addition to regulating transmitter release, Bassoon and Piccolo maintain synaptic integrity by reducing the proteasome- and autophagy-mediated degradation of presynaptic molecules (Waites et al., 2013; Okerlund et al., 2017; Hoffmann-Conaway et al., 2020; Montenegro-Venegas et al., 2021). At the electron microscopy level, the multimolecular complex of presynaptic scaffold proteins manifests as a meshwork of filamentous structures termed the presynaptic particle web (Phillips et al., 2001) or cytomatrix of active zones, i.e., CAZ (Cases-Langhoff et al., 1996; Garner et al., 2000; Dresbach et al., 2001).

Bassoon is a particularly large CAZ molecule, comprising 3,938 amino acids in the rat and 3,926 amino acids in humans (tom Dieck et al., 1998). It shares 10 regions of sequence homology with Piccolo/Aczonin (Wang et al., 1999; Fenster et al., 2000). Light microscopy super-resolution studies and electron microscopy studies have revealed that Bassoon and Piccolo are oriented in a particular way at synapses, with their C-termini closer to the active zone plasma membrane than their N-termini (Dani et al., 2010; Limbach et al., 2011). Thus, Bassoon and Piccolo appear to be extended proteins with a parallel orientation at synapses, consistent with the assumption that they may represent some of the filamentous CAZ structures observed by electron microscopy.

Using recombinant Bassoon constructs (Dresbach et al., 2003), we previously imaged the incorporation of Bassoon into nascent synapses and its turnover at existing synapses (Shapira et al., 2003; Bresler et al., 2004; Tsuruel et al., 2006, 2009). In the course of these studies, we also found that Bassoon, in addition to being a CAZ protein, is associated with the Golgi-apparatus, and that associating with the Golgi-apparatus is a prerequisite for the subsequent trafficking of Bassoon to synapses (Dresbach et al., 2006). Indeed, Bassoon, Piccolo, and ELKS/CAST/ERC are all detected at the Golgi apparatus and appear to exit the Golgi apparatus on transport vesicles that may carry CAZ material to synapses (Zhai et al., 2001; Maas et al., 2012). Unlike at synapses, the nanostructure of Bassoon at its second prominent subcellular localization, i.e., the Golgi-apparatus, has not been investigated. Here, we created a new generation of Bassoon constructs and determined their localization and arrangement at the Golgi-apparatus by stimulated emission depletion (STED) microscopy.

We found that Bassoon is an extended molecule at the *trans*-Golgi-network (TGN) with its N-terminus closer to the TGN than its C-terminus.

MATERIALS AND METHODS

Animals

Cells used in the study were obtained from bassoon gene trap (Bsn^{GT}) (Hallermann et al., 2010); mouse strains backcrossed over more than 10 generations to C57BL/6N. Bsn^{GT} mice were obtained from Omnibank ES cell line OST486029 by Lexicon Pharmaceuticals, Inc. (The Woodlands, TX, United States). All experiments involving rodents were performed in accordance with the European Committees Council Directive (86/609/EEC) and approved by the local animal care committees (Landesverwaltungsamt Sachsen-Anhalt, Germany, and the State Government of Lower Saxony, Germany).

Antibodies

The following antibodies were used for immunocytochemistry (IC): mouse anti-Bassoon (1:500 ENZO life systems), rabbit anti-Piccolo (1:200 Synaptic systems), mouse anti-TGN38 (1 to 500 BD-Transduction Laboratories), mouse anti-Syntaxin 6 (1:300 Abcam), chicken anti-GFP (1:3,000 Abcam), rabbit anti-GFP (1:1,000 Abcam), mouse anti-Synaptophysin (1:1,000 Sigma Aldrich), guinea pig anti-SHANK2 (1 to 1,000 Synaptic systems), Nanobodies: RFP-Booster-Atto594 and GFP-Booster-Atto647 (1:300 Chromotek), Mouse AlexaFluor[®]647 (1:1,000 for Epifluorescence microscopy), Chicken Cy5.5 (1:150 for STORM Jackson/Invitrogen), Chicken and Rabbit Alexa Fluor[®]488 (1:1,000 Invitrogen), STED dyes: Mouse Abberior Star Red and Mouse Atto594 (1:100).

Full-Length Bassoon Constructs

New full-length rat Bassoon constructs were created in the ampicillin-resistant pCS2⁺ vector backbone. They were designed to include either an intramolecular tag (mRFP or mGFP) near the N-terminus of Bassoon, or a C-terminal tag downstream of amino acid 3,938 of Bassoon, incorporating either mRFP or mGFP, or both tags. The intramolecular tag was created by gene synthesis in a way that its coding sequence, after insertion into the HindIII site of rat Bassoon, was preceded by amino acids 1–97 of Bassoon and was followed by amino acids 95–3,938 of Bassoon. We generated the G2A-mRFP-Bsn-mEGFP myristoyl mutant by inserting a point mutant at the second amino acid position, thereby replacing a glycine amino acid with alanine in the sequence of the full-length mRFP-Bsn-mEGFP construct. Overviews and details are presented in **Supplementary Figure 1**. The plasmid called “CFP-Golgi” (containing amino acids 1–81 of β -1,4-glycosyltransferase) was acquired from Clontech.

Primary Hippocampal Neuron Cultures

Rat cultures: E19 rat hippocampi were dissected as previously described (Dresbach et al., 2006). Hippocampi were dissociated by a 20-min trypsin treatment at 37°C and trituration. About

50,000 dissociated neurons/cm² were grown on poly-lysine-coated coverslips (Sigma Aldrich) in a Neurobasal medium enhanced with 2% B-27 and 0.5% L-Glutamine (ThermoFisher). Primary hippocampal neurons growing on either 12-mm or 18-mm coverslips, in 24-well or 12-well plates, respectively, were transfected with the Lipofectamine at day *in vitro* 3 (DIV3) and fixed, with 4% paraformaldehyde, for imaging of young neuronal cultures at day *in vitro* 7 (DIV7) or for mature day *in vitro* 14 (DIV14)-transfected cultures. The protocol for which was performed as described previously (Dresbach et al., 2006).

Mouse cultures were prepared as described (Montenegro-Venegas et al., 2021). Briefly, P0-P1 wild-type mice cortices were dissected to generate the feeder layer of a sandwich culture. Hemispheres of cortices with their meninges removed were chopped up in 4.5 ml of Hanks' Balanced Salt Solution (HBSS) and incubated for 15 min at 37°C in 2.5% trypsin [without Ethylenediaminetetraacetic acid (EDTA)]. These pieces were then washed in HBSS and dissociated in a glia medium that consisted of a 90% plating medium and 10% DNase (Invitrogen). Both hemispheres of one brain were dissociated in a 1-ml glia medium and plated in 10 ml of a plating medium that was identical to a rat primary culture plating medium. The medium was changed every 4–5 days, and the confluent glia were trypsinated, washed in HBSS, and 5 ml of the glia was plated on a 6-cm dish. Two P1 Bsn^{-/-} knockout mice and two wild-type Bsn^{+/+} littermates were prepped into dissociated primary hippocampal neurons, following the same protocol as was used for rat primary culture. About 50,000 hippocampal neurons in a 100- μ l volume were plated on coated 18-mm round glass coverslips. These coverslips were first incubated for 1 h at 37°C and 5% CO₂ and then transferred, neurons facing down, onto dishes containing the feeder layer of glia and 5 ml of a culturing medium [94% Neurobasal, 2% Glutamax (Invitrogen), 2% B27, 1% NaPyr (0.1 M), 1% Pen/Strep (0.1 M)]. These coverslips were left to grow at 37°C and 5% CO₂ and were treated with 2 μ l Ara-C (Sigma) on day *in vitro* 1 (DIV1) and DIV3 to prevent glia overgrowth and were fed one time a week with an exchange of 1 ml of a fresh culturing medium to maintain optimal growth of the culture.

Transfection

To visualize Golgi association of Bassoon constructs in hippocampal neurons (Figures 1, 3–6), we applied the Lipofectamine transfection method on DIV3 neurons and fixed them on DIV5–7 neurons with 4% paraformaldehyde, as previously described. Briefly, a conditioned medium of neurons, on 12-mm coverslips, was exchanged with a 500-ml pre-warmed Neurobasal medium, containing 2% B-27 and 1% of 2-mM L-Glutamine, saved and incubated along with the neurons for 20–30 min. A Lipofectamine solution and a DNA solution of 25- μ l OptiMem/well (Life Technologies) with 1 μ l of Lipofectamine 2,000/well (Invitrogen) and 1 μ g of plasmid DNA/well were prepared and mixed after 10-min room-temperature incubation. The Lipofectamine-DNA mix was further incubated for 20 min at room temperature; 50 μ l/well of the solution was dropwise applied on the neurons and incubated for 75 min in 37°C and 5% CO₂ conditions. The transfection was completed after three

pre-warmed Neurobasal washes and reinstating the transfected neurons in their conditioned medium at 37°C. These neurons were fixed the next day for 20 min in cold 4% paraformaldehyde solution before immunocytochemistry was performed.

Immunocytochemistry

Primary cultures of hippocampal neurons were washed multiple times after the paraformaldehyde fixation, blocked for 20 min with the primary antibody-buffer (10% FBS, 5% sucrose, 2% albumin, 0.3% Triton X-100 in 1 \times PBS) at room temperature, and stained with the primary antibodies, diluted in the primary antibody-buffer, overnight at 4°C. Following multiple washes, secondary antibody dilutions were prepared in the secondary antibody-buffer (0.3% Triton X-100, 5% sucrose, and 2% albumin in 1 \times PBS) and applied on the coverslips for 1 h, in darkness, at room temperature. Three washes of 1 \times PBS and one of distilled water were performed on the coverslips before being mounted on slides with DABCO-mowiol (Sigma) and left to dry overnight.

Microscopy and Analysis

Epifluorescence Microscopy

An inverted Zeiss fluorescence microscope (Observer.Z1) with a Photometrics CoolSnap HQ2 camera (Tucson, AZ, United States) was used to image samples at a magnification of 40 \times and 63 \times . The following filters from AHF were used: F46-000 for DAPI, F46-002 for GFP and Alexa 488, F46-004 for Atto594 and Alexa 546 dyes, and F46-006 for AttoKK1212 and Alexa 647. Exposure times of 500 ms for F46-002 and F46-004 filters and 1,000 ms for the F46-006 filter were applied. The images were processed with the ImageJ software (NIH)¹ to generate scale-bar-inserted RGB-merged TIFF files for further analysis with Imaris Measurement Pro software (Bitplane AG, Zürich, Switzerland). Images in Figure 1 and Supplementary Figure 1 were adjusted for brightness and contrast in ImageJ, where needed, calculated, and stamped with a suitable sized scale bar.

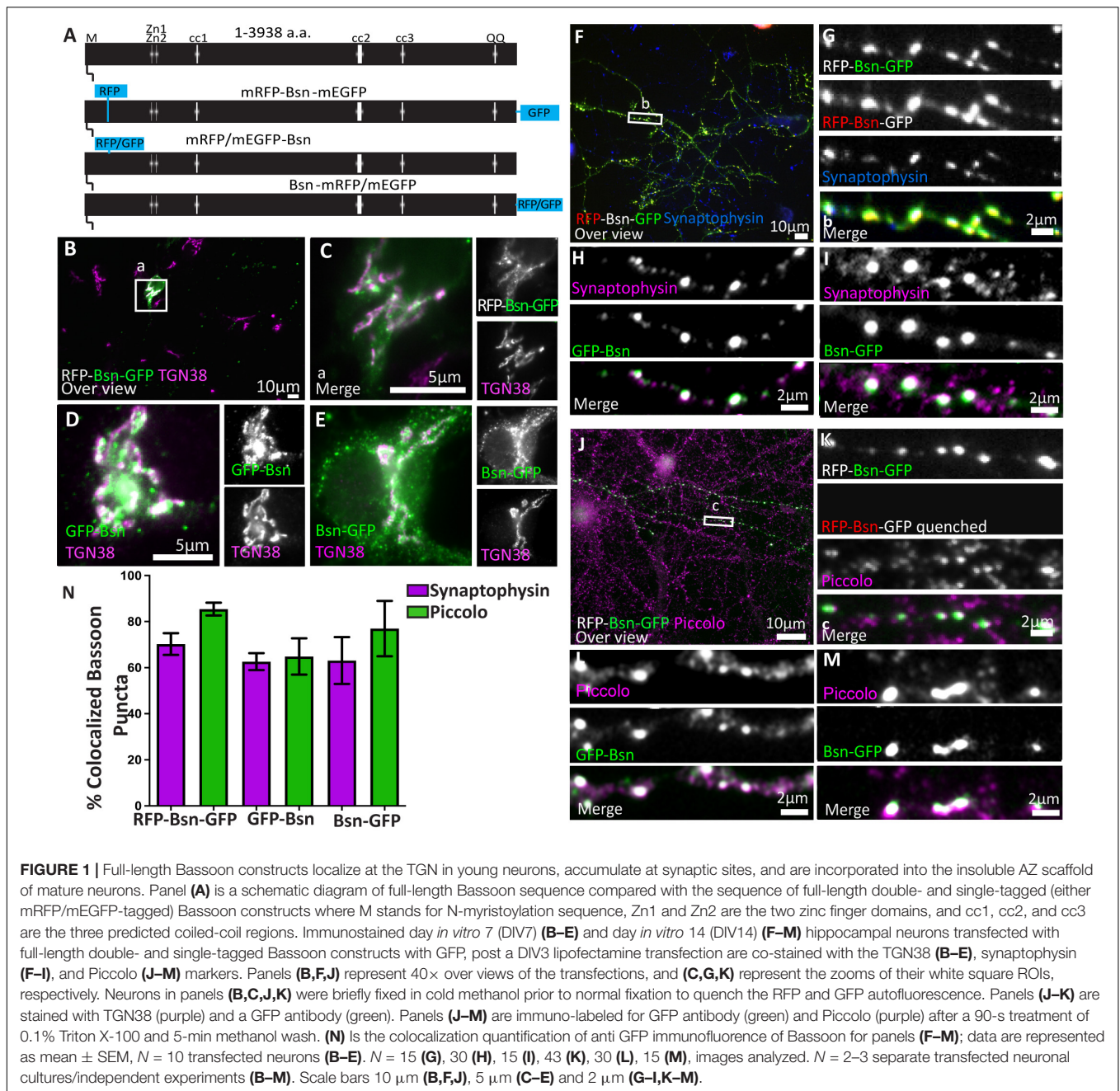
Colocalization Analysis for Conventional Epifluorescence Images

Merged multichannel 40 \times light microscopy images were analyzed using MetaMorph Offline Version 7.7.0.0 (Molecular Devices, Inc., San Jose, CA, United States). A threshold is set for each channel followed by the generation of a mask for all channels in three areas of size 25 pixels long (representing 2 μ m in the sample) and 4 pixels wide, per image. These area masks were then overlaid in the arithmetic tool and divided to generate a third mask containing only the population of fluorescence signals in the mask that do colocalize. The amount of bassoon colocalized is represented as a percentage of the bassoon-colocalized population divided by the total bassoon population.

Stimulated Emission Depletion Microscopy

Stimulated emission depletion images in Figures 3–6 and Supplementary Figures 3–5 were acquired on a custom-built two-color STED microscope that includes a 1.4 NA 100 \times objective (PL APO HCX 100 \times 1.4–0.7 Oil, Leica Microsystems, Wetzlar, Germany), and a 775-nm STED laser

¹imagej.nih.gov/ij/



(ELP-5-775-DG, IPG Photonics Corporation, Oxford, MA, United States). The dyes were excited at wavelengths of 470, 595, and 640 nm, while the fluorescence was detected with avalanche photodiodes from 500–550 nm, 600–640 nm, and 660–720 nm, respectively. Corroborative confocal images were acquired using a LED illumination source, a monochrome filter, and a camera (DMK41 AU02, The Imaging Source). The LED illumination source for such overview images was manually installed every session, wherein a 590-nm LED was installed with the 700/60 fluorescence filter, and a 640RDC dichroic filter or a 490-nm LED was installed (upon requirement) with the 450/60 fluorescence

filter in the camera path. Images were taken at 300- to 700-mW STED power, 4-μW excitation power, dwell time of 30–100 min and a pixel size of 10 nm. **Figure 2** and **Supplementary Figure 4** were acquired on a Abberior QuadSCAN two-color STED microscope. The setup was equipped with a pulsed 775-nm STED laser and two pulsed excitation laser sources at 594 and 640 nm integrated into an Olympus IX83 microscope. The setup also included a 100 × 1.4NA objective; a four-color LED illumination source, a gated avalanche photodiode (APD), and a wide monochrome field. A pixel size of 10 nm, dwell time of 3 min, and three-line accumulations were applied to the images.

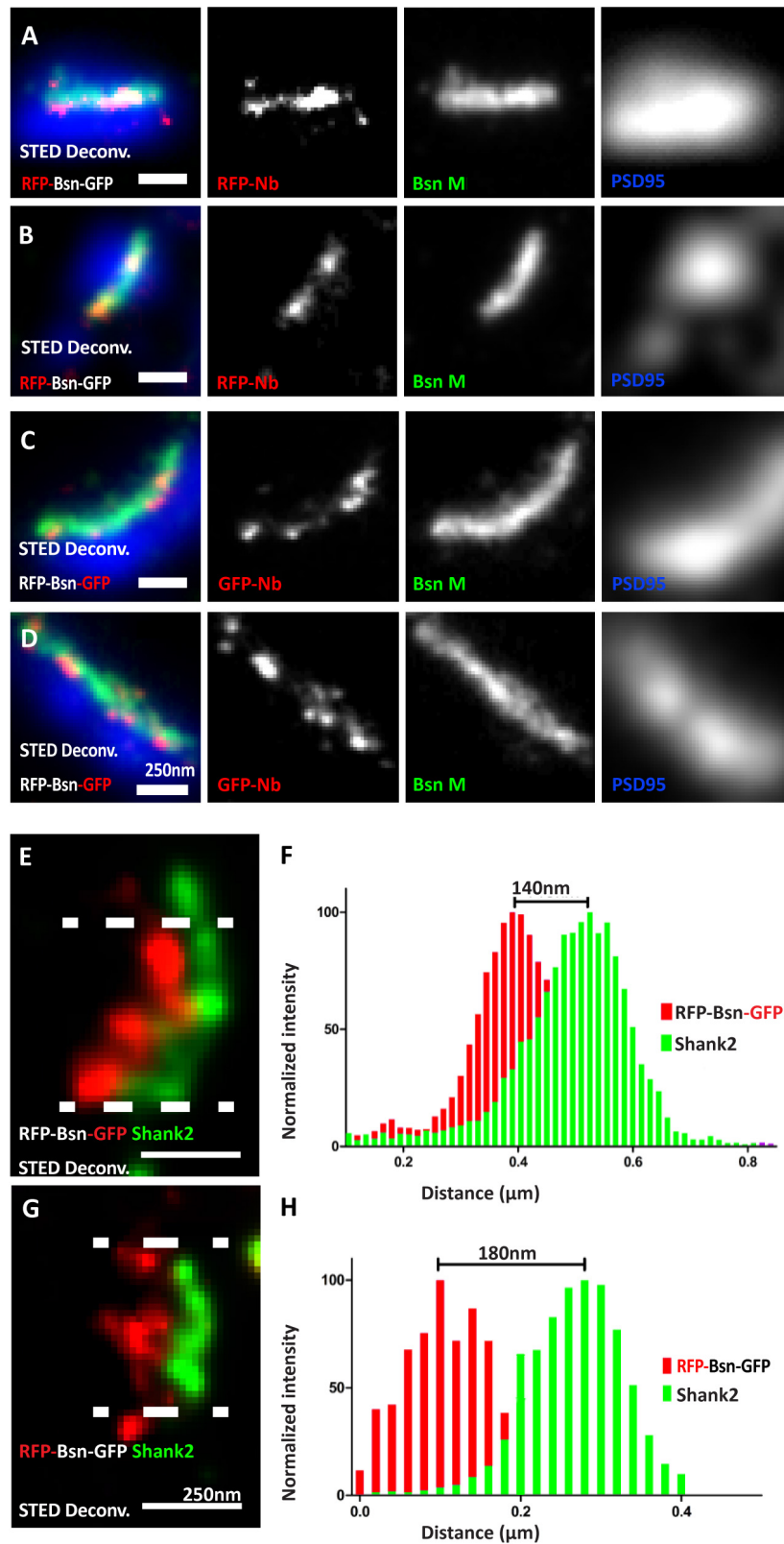


FIGURE 2 | Visualizing the termini of full-length mRFP-Bassoon-mEGFP and its orientation with nanobodies at mature synaptic sites. Day *in vitro* 14 mass hippocampal cultures transfected with the mRFP-Bassoon-mEGFP construct and imaged using two-color STED microscopy. The construct was visualized at (Continued)

FIGURE 2 | synaptic sites with postsynaptic scaffold markers PSD95 and Shank2, using either the RFP-nanobody-Atto594 to visualize the RFP tag and the N-terminus of the Bassoon construct (**A,B,G**)/the GFP-nanobody-Atto594 to visualize the GFP tag and the C-terminus of the Bassoon construct (**C–E**). Panels (**A–D**) are two-color-STED deconvolved (Deconv.) images of triple-color staining that label the endogenous presynaptic Bassoon signals with a traditional monoclonal antibody, nanoclusters of nanobody signals within the endogenous presynaptic Bassoon signals, and postsynaptic scaffold marker PSD95 (in a confocal mode). Panels (**E,G**) show the localization of nanobody-labeled C- and N-termini of mRFP-Bassoon-mEGFP and Shank2 in side-view images of its synapses. Distribution of localization points within a 350-nm thick line profiles at the center of the synapse (as shown by the area within the dashed lines) was measured, fit with gaussian distributions, and is plotted in panels (**F**) (C-terminus of tagged Bassoon and Shank2) and (**H**) (N-terminus of tagged Bassoon and Shank2). The distance between centroids of the two Gaussians defines the Bassoon-Shank2 distances. $N = 10$ transfected neurons (**A–H**) from which 14 (**E,F**) and 13 (**G,H**) side-view synapses analyzed as technical replicates. $N = 3$ separately transfected neuronal cultures/independent experiments (**A–H**). Scale bars 250 nm (**A–G**).

The resolution regularly obtained on both setups for Atto594 antibodies was 25–40 nm and, for Abberior Star Red antibodies, was 20–35 nm (at 300- and 700-mW STED-power, respectively). All raw double-channel STED images were acquired with the ImSpector Software (Max Planck Innovation, Munich, Germany and Abberior Instruments, Göttingen, Germany) and were processed using the Richardson – Lucy deconvolution function. During the deconvolution processing, a 2D Lorentz function, that fits the full width at half maximum (FWHM) fitted of the point spread function of each individual channel/image to the resolution estimate was used. The point spread function was automatically computed with a 2D Lorentz function having a FWHM of 20 nm, based on measurements with 20-nm crimson beads. Default deconvolution settings of 15 consecutive iterations were applied to reduce background noise. Images were not post-processed before quantification but exclusively afterward and only for brightness and contrast with ImageJ software (NIH) for visualization purposes. **Supplementary Figure 5** can be referred to for visualization of the raw and deconvolved STED data used in **Figures 4, 5**. Quantification and analysis were performed using Imaris Measurement Pro.

Quantitative Analysis of the Probability and Amount of Colocalization and the Distribution of Bassoon Constructs at the Golgi

Merged TIFF epifluorescence images or STED images were analyzed using Imaris Measurement Pro 8.1 (Bitplane AG.) software to ascertain the probability of colocalization (Pearson's correlation coefficient), amount of colocalization, and distribution pattern of signals within the images.

Soma images in **Figures 3–6** were analyzed within a ROI, generated by a freehand drawn mask, to exclude any signals in the image that was in the nucleus, outside the cell soma, or in a neighboring neuronal process. Images were analyzed for the probability of colocalization through the Imaris Coloc module (Bitplane AG). The integrated Costes P -value approximation plugin, within the Imaris Coloc module, first generates automated thresholds for all the channels of all the images, which are subsequently used to calculate the colocalization Pearson's correlation coefficient constants in the picture.

The amount of colocalization and distribution pattern of signals was calculated after Imaris Spots generation (Bitplane AG). Imaris Spots, a built-in spot detection algorithm, was used to generate objects for every punctuate signal, for all channels, in the images. These spot objects were defined by the automated intensity threshold value for each channel (calculated by the

Costes P -value approximation), signal diameter size range (10–160 nm for STED images and >200 nm for light microscopy images), and automated splitting of signal clusters (defined as >120 nm for STED images and >400 nm for light microscopy images) for each channel.

The amount of colocalization was calculated using Spots Colocalize, a MATLAB extension in the Imaris Spots module, at a distance threshold of 0–100 nm (for STED images) and 0–350 nm (for light microscopy images) from the spot centers.

The distribution pattern of AZ protein signals at the Golgi was extracted by applying the distance transformation MATLAB extension from the Imaris XT module to the spots object information generated *via* the Imaris Spots module. This distance transformation extension was applied on the Golgi label channel, transforming the Golgi voxel intensity data into spot coordinates. These spot coordinates were then used to calculate the shortest distance of each AZ protein spot object to the object border of a Golgi-label spot. The data for the shortest distances between all the AZ protein signals and the border coordinates of the Golgi-label and the total number of AZP signals within 0–100 nm or 101–1,000-nm distance ranges were extracted from the statistics of the Imaris Spot module, statistically tested, and graphically represented with GraphPad Prism (GraphPad Software, Inc., San Diego, CA, United States).

The distribution pattern of Bassoon constructs in **Figure 7A** was generated in GraphPad Prism and graphically visualized as violin plots, with a signal size upper limit of 600 nm to clearly represent the distribution and permit visualization of the median and interquartile ranges of the data. The average distance of each cell per set, in **Figure 7B**, was extracted from the Imaris Spots statistics and limited to the 220-nm cut-off was plotted in GraphPad Prism.

Quantitative Analysis of Distances Between Bassoon's Termini and the Post Synapse

All acquired light microscopy images were processed and visualized using ImageJ (see text footnote 1) and/or STED images with ImSpector software (Max-Planck Innovation). Line profiles were measured with ImageJ software along 350-nm-thick line profiles. Inter-peak Bassoon-SHANK2 distances were determined after fitting a Gaussian distribution in GraphPad Prism (**Figure 2**).

To factor out the effect of the varying number of signals counted per size of a hand-drawn mask in each image, the area in μm^3 of the mask used was divided by the signals measured per image.

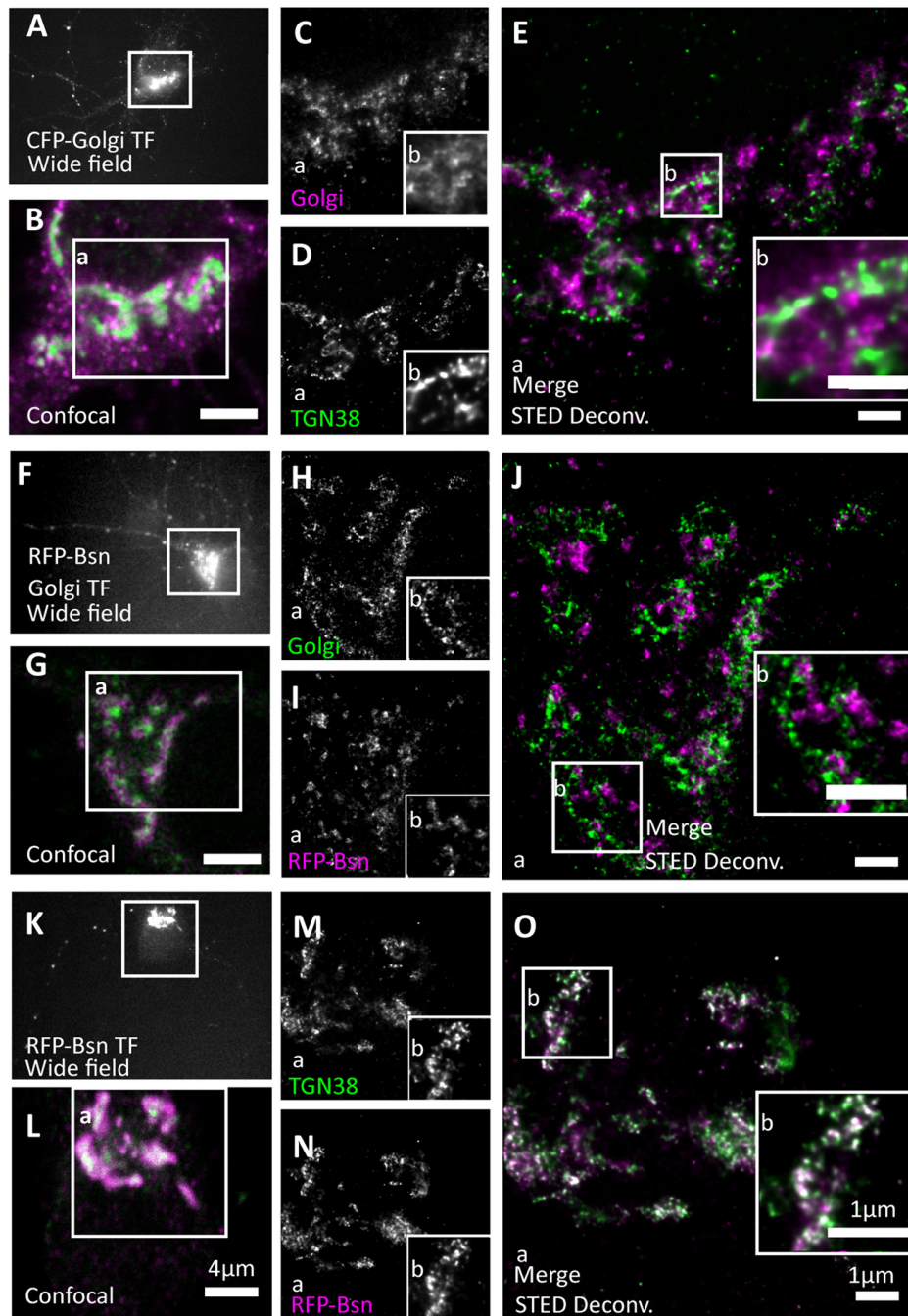
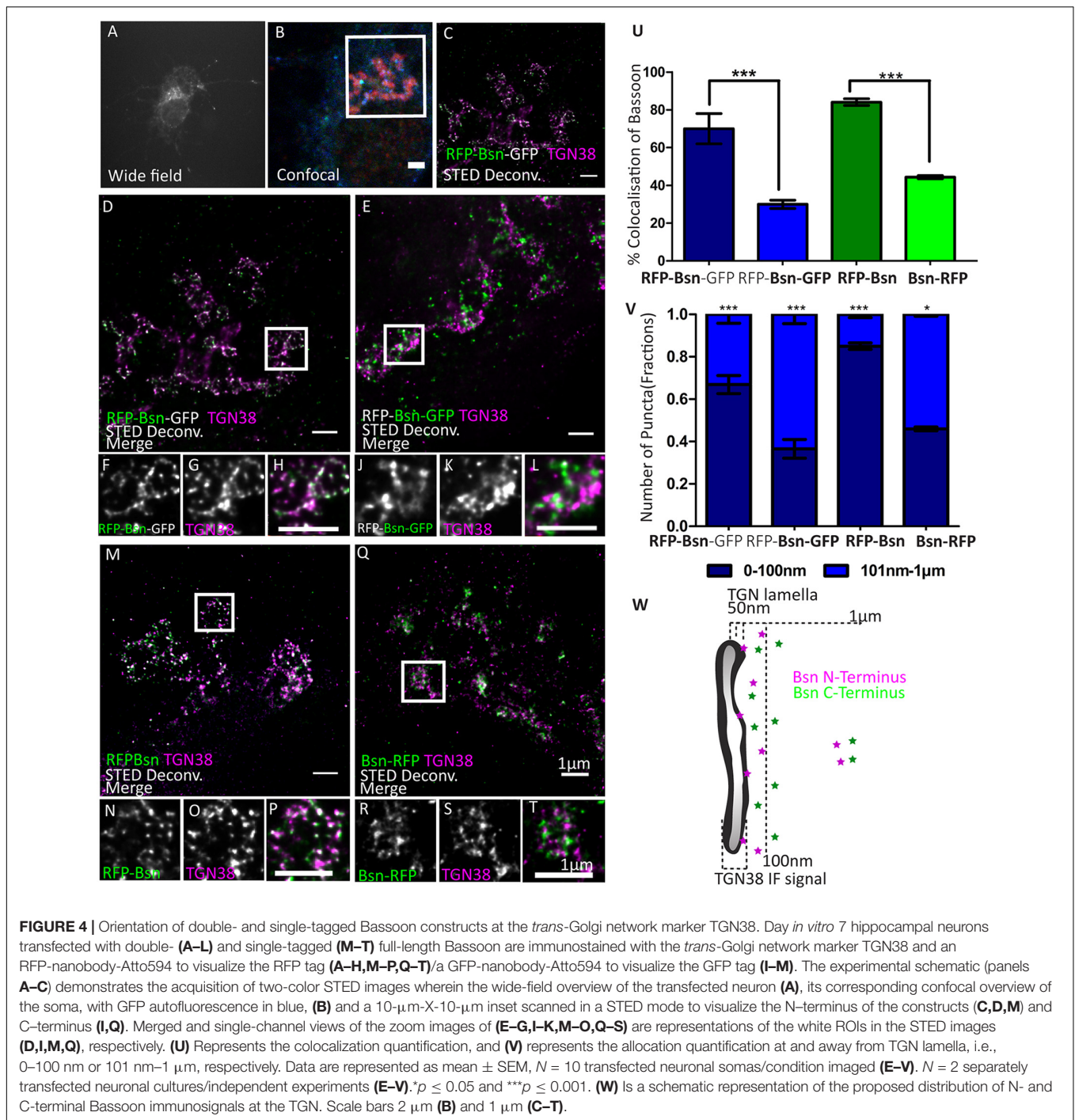


FIGURE 3 | Full-length Bassoon localizes to the *trans*-Golgi network, not the *trans*-Golgi sub-compartment. Day *in vitro* 7 hippocampal neurons were transfected with CFP-Golgi (a *trans*-Golgi sub-compartment maker), full-length single-tagged mRFP-Bsn construct, and immunostained using GFP and/or RFP nanobodies against tagged constructs and from (A–E) with TGN38 (a *trans*-Golgi network maker). Two-color STED images of both Golgi sub-compartment markers (A–E), CFP-Golgi and RFP-Bsn constructs (F–J), and RFP-Bsn at TGN38 (a *trans*-Golgi Network maker) (K–O). (A,F,K) Show wide field overview of transfected construct, (B,G,L) the confocal zooms of the soma, inset **a** reflects the single channels and merged full STED-deconvolved (Deconv.) images of (C–E,H–J,M–O), while inset **b** represents the zooms of STED images. $N = 10$ transfected neurons per condition imaged in total, per trasfection 5 individual-transfected soma/condition, were imaged as technical replicates (A–O). $N = 2$ separately transfected neuronal cultures/independent experiments (A–O). Scale bars 4 μm (B,G,L) and 1 μm (E,J,O).

Statistics

Statistical analysis and representation of all resultant data were prepared in GraphPad Prism 5.02. For Figures 1–6 and

Supplementary Figure 4, a one-way ANOVA with the Tukey's multiple comparisons test was performed between pairs of relevant data sets.



As the data in Figure 7 is not normally distributed, to show an overall difference in Bassoon signal distribution from the TGN lamella, we performed individual Kolmogorov – Smirnov distribution comparisons between pairs of conditions.

For Figures 1–7 and Supplementary Figure 4, data are presented as mean \pm SEM, and statistical differences were considered significant, strongly significant, and extremely significant at respective p values of * $p < 0.05$, ** $p \leq 0.01$, *** $p \leq 0.001$, and **** $p \leq 0.0001$.

RESULTS

Characterizing Second-Generation Full-Length Bassoon Constructs

We first aimed at improving three features of recombinant Bassoon:

- Faithful expression of the full-length protein, including its C-terminal tag: when expressed in neurons,

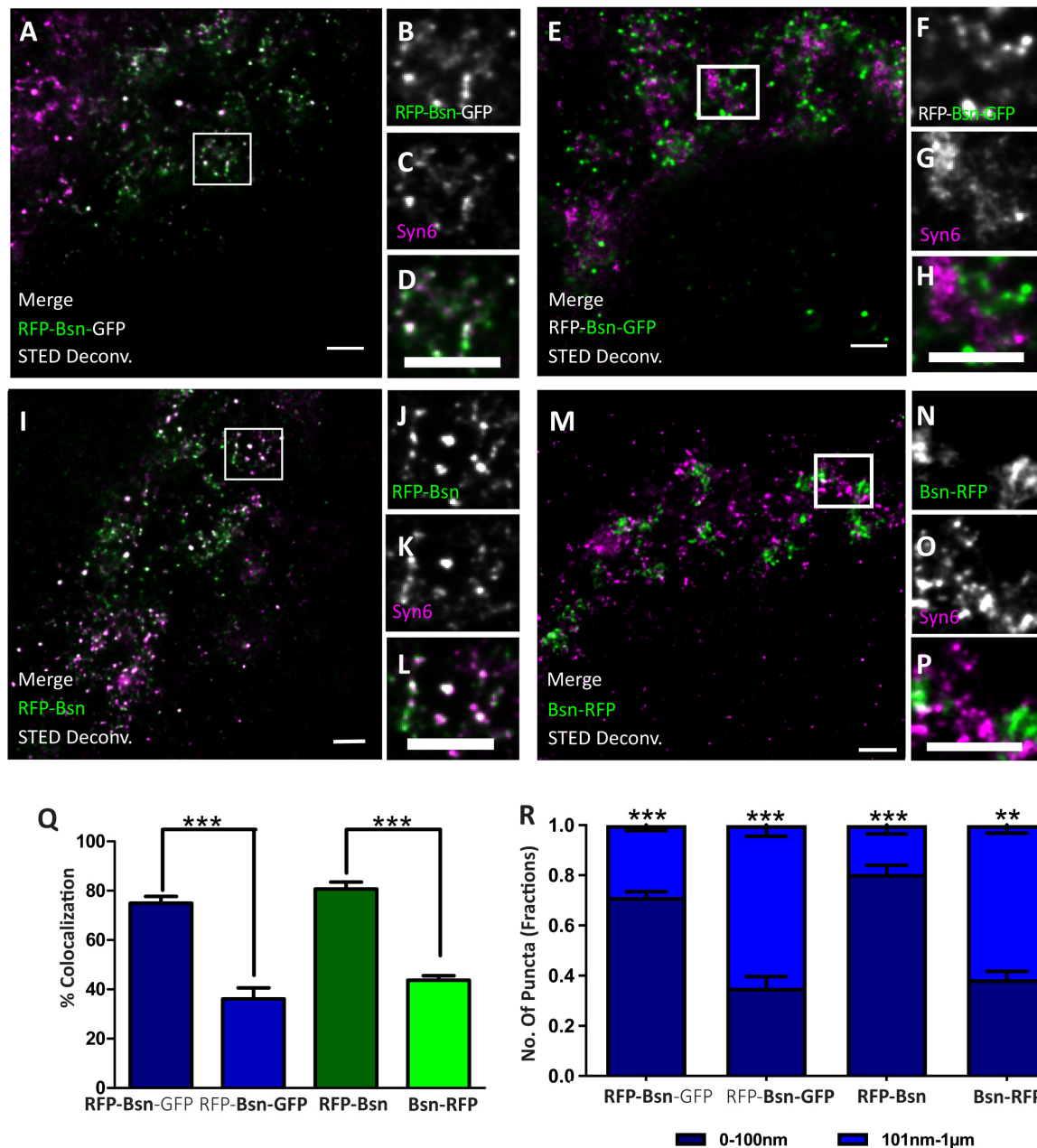


FIGURE 5 | Orientation of double- and single-tagged Bassoon constructs at the *trans*-Golgi network marker Syntaxin 6 (Syn6). Transfected DIV7 hippocampal neurons immunostained for either one or both termini of full-length Bassoon with RFP-nanobody-Atto594/GFP-nanobody-Atto647 and the Syn6 marker. Two-color, deconvolved, 10- μ m-X-10- μ m STED images and their ROI zooms show double-tagged and single-tagged Bassoon constructs in panels (A–D,I–L) (of which the N-termini of constructs were imaged) and panels (E–H,M–P) (of which the C-termini of the constructs were imaged), respectively. Graph (Q) quantifies the amount of Bassoon colocalization with Syn6, and graph (R) quantifies the Bassoon signal allocations at and away from TGN38 lamella, i.e., 0–100 nm or 101 nm–1 μ m, respectively. Data are represented as mean \pm SEM, $N = 10$ transfected neuronal somas/condition imaged and $N = 2$ separate transfected neuronal cultures/independent experiments (A–R). Statistically tested with a Tukey's multiple comparison $**p \leq 0.01$ and $***p \leq 0.001$. Scale bars 1 μ m (A–P).

Bassoon-1-3938-EGFP, in addition to producing punctate synaptic fluorescence signals, also produces diffusely distributed green fluorescence, presumably resulting from soluble EGFP or a soluble C-terminal fragment of Bassoon with the EGFP-tag attached (Dresbach et al., 2003). We realized serendipitously that this diffusely distributed

green fluorescence also occurred when the EGFP-coding sequence was attached out of frame to the 3' end of Bassoon, suggesting that a cryptic ribosomal entry site exists somewhere near the 3'-region of Bassoon or in the linker located between Bassoon and EGFP. To prevent translation of the C-terminal EGFP-tag, we changed the

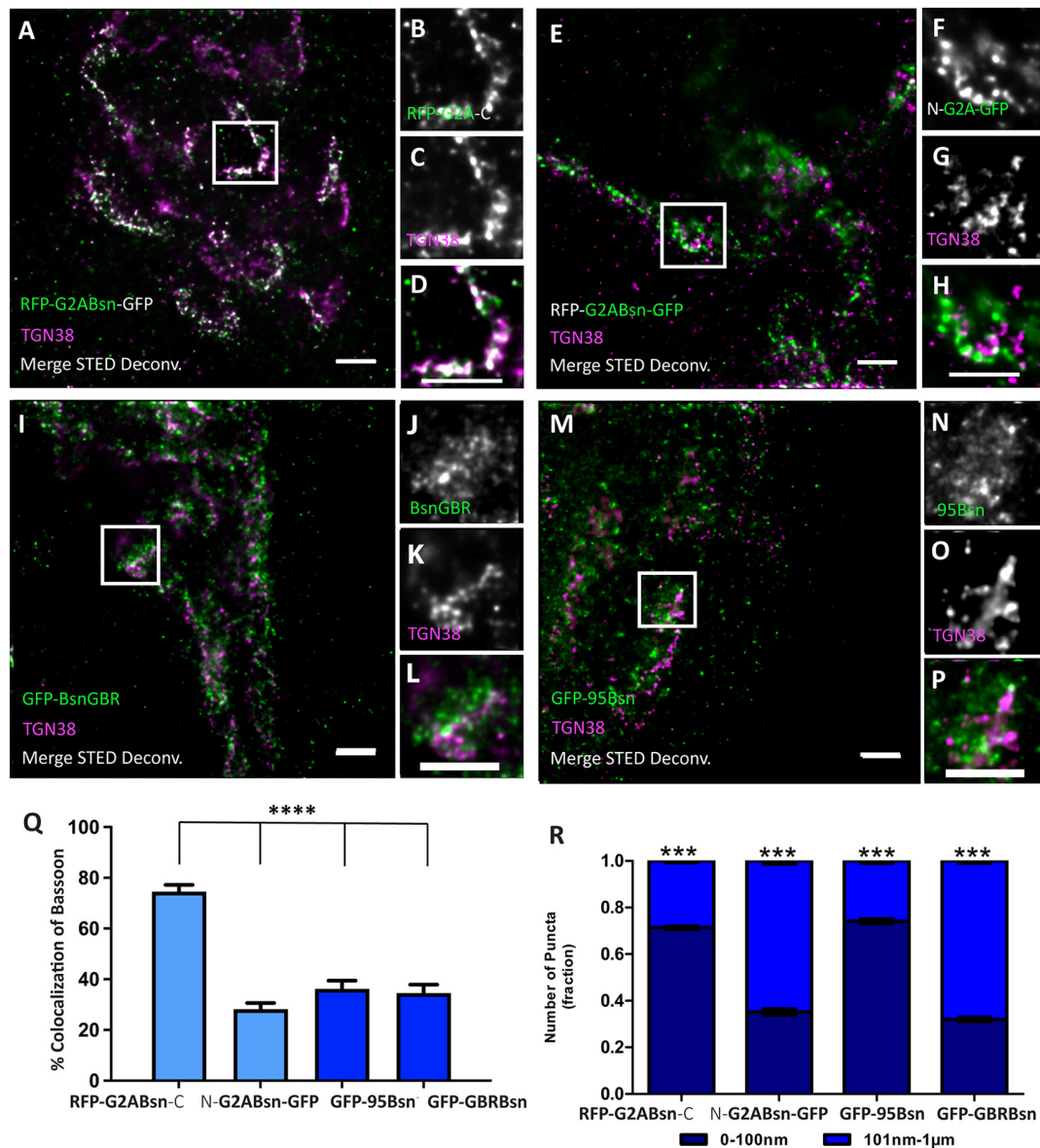


FIGURE 6 | Orientation of deletion constructs of Bassoon at the *trans*-Golgi network. Day *in vitro* 7 hippocampal neurons transfected with tagged Bassoon deletion constructs a myristoyl group-deficient G2A-mRFP-Bsn-mEGFP (**A–H**), Bassoon’s N-terminus, i.e., (95–3938) 95-Bsn construct (**I–L**), and Bassoon’s N- and C-termini (2088–2038), i.e., Bsn-GBR construct (**M–P**), were visualized with GFP-nanobody-Atto647/RFP-nanobody-Atto594 and a TGN38 marker. Insets of the two-color STED-deconvolved images in (**A,E,I,M**) are represented in panels (**B–D,F–H,J–L,N–P**), respectively. Graphs (**Q,R**) quantify the colocalization and signal allocations of Bassoon at the TGN38, respectively. Data are represented as mean \pm SEM, $N = 8$ transfected neuronal somas/condition imaged and $N = 2$ separate transfected neuronal cultures/independent experiments (**A–R**). Statistically tested with a Tukey’s multiple comparison test. *** $p \leq 0.001$ and **** $p \leq 0.0001$. Scale bars 1 μm (**A–P**).

linker sequence and removed the start ATG from the EGFP-coding sequence.

- (b) The accessibility of its N-terminus: Bassoon contains a functional consensus site for N-myristoylation (Dresbach et al., 2003), so N-terminal tags might impair N-myristoylation. Ideally, a tag designed to locate the N-terminal region of Bassoon should be placed downstream of the N-myristoylation consensus site. To leave this consensus site unaffected, we placed either

RFP, CFP, or GFP as intramolecular tag 97 amino acids downstream of the N-terminus of Bassoon, using an endogenous HindIII site in the rat Bassoon cDNA. We will refer to these tags as “intramolecular N-terminal” tags to highlight both of their features, i.e., leaving the very N-terminus intact, and placed close to it.

- (c) Its tendency to aggregate: Bassoon may form homodimers, and heterodimers with Piccolo (Maas et al., 2012). Tags with an inherent capacity to dimerize could cause aberrant

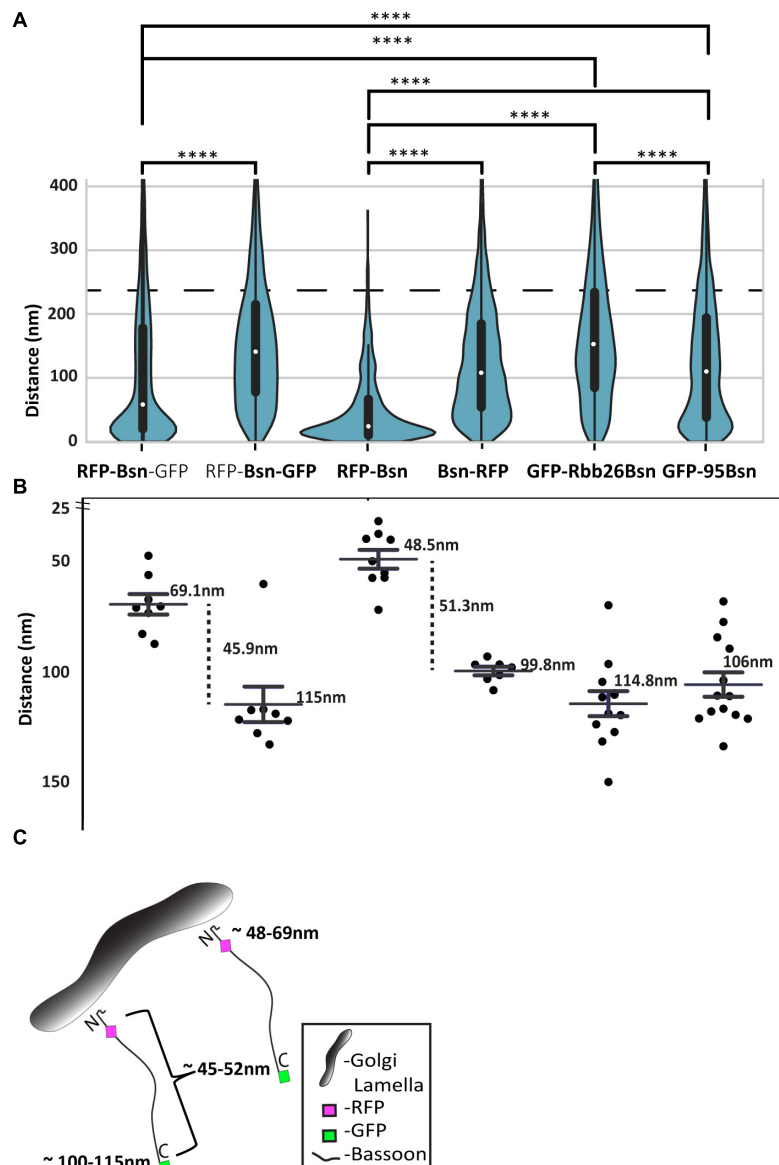


FIGURE 7 | Distribution and average distances of all full-length and mutant Bassoon signals from the TGN38 reference marker. Bean plots in panel (A) display all signal distributions of single- and double-tagged full-length and deletion constructs of Bassoon from their nearest TGN38 marker. The light gray lines within each individual bean plot show individual observations of Bassoon signals. The blue ROI represents the 220-nm range that corresponds to 75% of the total Bassoon signals oriented around the TGN lamella (A). Pairs of distributions were compared by a Kolmogorov–Smirnov test **** $p \leq 0.001$. The average distances of the Bassoon tags of all five constructs within the 200-nm distance range are plotted in (B). (C) Is a schematic diagram that shows the average distance N and C-termini of full-length Bassoon molecules possess at the TGN lamella.

oligomerization and generate non-functional aggregates of Bassoon. To prevent this, we used monomeric fluorescent proteins, including RFP, CFP, and the A207K variant of EGFP. We use the term “EGFP” when referring to previously generated constructs, which harbor standard EGFP, and we use the term “GFP” when referring to new constructs, which harbor the monomeric variant. A schematic synopsis of the new constructs is presented in **Figure 1A**, and additional information on their design is depicted in **Supplementary Figure 1**.

To test the new constructs, we transfected dissociated rat hippocampal cultures with the new full-length single-tagged and double-tagged Bassoon constructs on Day 3 after plating (DIV3). We characterized the subcellular localization of these Bassoon constructs in young (DIV7) and mature (>DIV14) neurons (**Figure 1**) by immunostaining fixed cultures using a single-domain antibody (nanobody) directed against RFP, a polyclonal antiserum directed against GFP, and monoclonal or polyclonal antibodies directed against markers for subcellular structures. **Figure 1** shows the results for the two GFP-tagged constructs and

for the dually tagged construct. The results for the RFP-tagged constructs are depicted in **Supplementary Figure 3**.

In the soma of young neurons, all constructs were readily detected at the Golgi apparatus, labeled by the *trans*-Golgi-network (TGN) transmembrane protein TGN38 (**Figures 1B–E**). Previous reports observed similar localizations of endogenous and recombinant Bassoon signals in young neurons (Dresbach et al., 2006; Maas et al., 2012). To test the targeting of these constructs to synapses and their incorporation into the CAZ matrix, we analyzed their localization in mature neuronal cultures. In DIV14 neurons immunostained for the tags and the synaptic vesicle marker synaptophysin or the CAZ marker Piccolo, none of the constructs showed the diffusely distributed green fluorescence associated with the first-generation Bassoon-EGFP (Dresbach et al., 2003) and all of the constructs accumulated at synaptic sites (**Figures 1F–N**). The degree of colocalization with synaptophysin was 70.25% ($\pm 18.23\%$ SD) for the dually tagged construct, 66.7% ($\pm 12.9\%$ SD) for mRFP Bassoon, and 62.64% ($\pm 6.37\%$ SD) for Bsn-mRFP (**Figures 1F–I, N** and **Supplementary Figure 2**). Likewise, these Bassoon accumulations colocalized with the core CAZ scaffold protein Piccolo (**Figures 1J–N** and **Supplementary Figure 2**), further corroborating their localization to synapses. This was true for the dually tagged ($85.4 \pm 18.42\%$ SD) and the single-tagged Bassoon constructs ($69 \pm 5.6\%$ SD for mRFP-Bsn and $76.97 \pm 10.16\%$ SD Bsn-mRFP).

Active zone proteins become resistant to Triton X-100 extraction once they became incorporated into the CAZ scaffold (Dresbach et al., 2003). When we applied a 0.1% Triton X-100 extraction to live neurons, followed by fixation and immunostaining for the tags and for endogenous Piccolo, we found that the synaptic accumulations of the recombinant proteins were, indeed, preserved. Colocalization with Piccolo was 85.43% ($\pm 18.42\%$ SD) for the dually tagged Bassoon, 64.85% ($\pm 15.74\%$ SD) for GFP-Bsn, and 76.97% ($\pm 24.1\%$ SD) for Bsn-GFP. The resistance of the recombinant Bassoon to the Triton X-100 treatment is indicative of its successful incorporation into mature active zone scaffolds (**Figures 1J–N**).

Visualizing the Orientation of Full-Length Bassoon Constructs With Nanobodies and Super-Resolution Imaging

We then employed these constructs to study recombinant Bassoon by STED nanoscopy. To take full advantage of super-resolution microscopy, we used camelid antibodies, called nanobodies, to detect the tags. These anti-mRFP and anti-mEGFP nanobodies are small (1.5 nm \times 2.5 nm) single-domain molecules derived from one heavy chain of an alpaca IgG antibody (Hamers-Casterman et al., 1993). They are designed to identify a single epitope on the tertiary structure of mRFP and mEGFP fluorophores (5-nm diameters). These nanobodies were pre-coupled to two molecules of organic ATTO-TEC dyes, each 2–3 nm in size. The mRFP nanobody was coupled to ATTO594; the mEGFP nanobody was coupled to ATTO647. Compared with traditional primary and secondary antibodies, which create a 30-nm labeling distance from the epitope site, the nanobody-ATTO

dye complex generates a three-times-smaller-label cloud around the tags (Harris et al., 1998; Wildanger et al., 2009a,b; Ries et al., 2012).

Our microscopy setup allowed us to record triple-immunofluorescence images, with two dyes recorded in a STED mode at a resolution of 20 nm, and a third dye recorded in a confocal mode. In the first set of experiments, we analyzed cultures transfected with dually tagged Bassoon, asking three questions: (1) Do the nanobodies allow for detection of the construct in the STED mode? (2) Can we spatially resolve the N- and the C-terminus of the dually tagged construct? (3) If so, is the recombinant construct oriented as predicted, i.e., with the C-terminus closer to the active zone than the N-terminus (Dani et al., 2010)?

Both the RFP-nanobody and the GFP-nanobody produced line-shaped or crescent-shaped signals (**Figures 2A–D**), as expected for the appearance of active zone-associated proteins at super-resolution (Dani et al., 2010). To make sure that what we analyzed represented synaptic Bassoon, we only analyzed signals fulfilling two criteria: they had to be line shaped or crescent shaped, suggesting that they represent side-view synapses, and in addition, they had to colocalize with postsynaptic marker PSD95 immunofluorescence recorded in the confocal mode, corroborating that these signals represent synaptic Bassoon (**Figures 2A–D**). Comparing the nanobody signals to signals produced by a conventional monoclonal antibody directed against amino acids 756–1,001 of Bassoon and detected by secondary antibodies revealed that the nanobody signals and the indirect immunofluorescence signals colocalized when analyzed by dual-color STED microscopy. In addition, the nanobody signals produced sub-clusters of fluorescence within the lines and crescents (**Figures 2A–D**). This is consistent with the assumption that their small size and their direct coupling to the fluorescent dyes allow for greater detection precision compared with indirect immunofluorescence with a conventional antibody. Overall, these data indicate that the RFP- and GFP-nanobodies can localize the N- and C-terminus of recombinant Bassoon molecules within the CAZ of mature neurons, and that the spatial precision of detection at least equals, and may exceed, the spatial precision provided by indirect immunofluorescence using a conventional antibody.

The orientation of endogenous Bassoon at synapses in brain sections was previously analyzed using conventional antibodies imaged by Stochastic Optical Reconstruction Microscopy, a.k.a. STORM (Dani et al., 2010; Held et al., 2020). These studies used the monoclonal antibody to detect amino acids 756–1,001 and/or a polyclonal antibody against the C-terminal 330 amino acids of Bassoon. They showed that Bassoon molecules possess an extended conformation within the CAZ scaffold and are oriented with their C-termini closer to the synaptic cleft than their N-termini. Using our dual-color STED setup, we tested whether our constructs adopt a similar orientation in cultured neurons. We found that they, indeed, possess a similarly extended conformation, with the C-terminus 140 nm and the N-terminus 180 nm from the postsynaptic scaffold marker Shank2 (**Figures 2E–H**). These constructs, in combination with nanobodies and STED microscopy, therefore, form an effective

toolbox to visualize the nanoscopic localization and orientation of recombinant Bassoon in neurons.

Visualizing the Orientation of New Full-Length Bassoon Constructs at the Golgi-Apparatus

How Bassoon is arranged at subcellular sites other than synapses has not been investigated by nanoscopy thus far. Bassoon may form primordial scaffolds at the level of the Golgi-apparatus (Dresbach et al., 2006; Maas et al., 2012). To arrive at a more comprehensive understanding of the possible arrangement of Bassoon, we used STED microscopy to determine the localization and orientation of our new constructs at the Golgi-apparatus of immature neurons at DIV7.

We began by testing which Golgi compartment recombinant Bassoon is located to. The Golgi compartment is polarized across the flat stacks of cisternae/lamellae that form sub-compartments at its *cis* side, which receives materials from the endoplasmic reticulum (ER), and the *Trans* Golgi (TG) side, which sends them forward to their destinations. Additional vesicular-tubular structures both on the *cis* and *trans* ends of the Golgi stack are known to form specialized compartments for cargo sorting at the entry and exit sides of the Golgi. The *trans*-Golgi network (TGN) is a post-Golgi compartment, following the TG sub-compartment that is involved in complex cargo sorting mechanisms (Griffiths and Simons, 1986; Mellman and Simons, 1992). We identified the TG sub-compartment and its neighboring compartment the TGN separately and compared the extent of co-localization of Bassoon at these two substructures in the soma of cultured neurons. To label the TG sub-compartment, we expressed a CFP-tagged construct (named CFP-Golgi), containing the cytoplasmic domain of β -1,4-galactosyltransferase-11, which labels the last Golgi cisterna of the *trans*-Golgi compartment (Wittenmayer, 2014). To label the TGN, we immunostained for the marker TGN38. We detected recombinant constructs using the nanobodies, and we detected TGN38 using conventional primary and secondary antibodies. STED imaging revealed that the signals for the TG sub-compartment and TGN can be resolved and occupy different localizations in the soma (Figures 3A–E). mRFP-Bsn displayed virtually no colocalization with CFP-Golgi-labeled TG lamellae (Figures 3F–J) but colocalized extensively with TGN38 (Figures 3K–O), indicating that this construct is more closely associated with the TGN lamella than with the TG sub-compartment lamellae.

We then sought to determine the localization – and possibly the orientation – of Bassoon at the TGN in more detail. We first imaged the double-tagged Bassoon construct (RFP-Bsn-GFP) in somas of DIV7 neurons labeled with TGN38. The intramolecular N-terminal tag of the construct colocalized more extensively with TGN38 than its C-terminal tag (Figures 4A–K). On average, 67.5% (\pm 12.5% SD) of the signals coming from the intramolecular N-terminal tag but only 29.8% (\pm 7.7% SD) of the signals coming from the C-terminal tag colocalized with TGN38 (Figure 4T). To rule out that the difference could be caused by different avidities of the RFP

and the GFP nanobodies, we transfected neurons either with RFP-Bsn or with Bsn-RFP and detected the tags of both constructs using the RFP nanobody. Again, the intramolecular N-terminal tag colocalized more extensively with TGN38 than the C-terminal tag (Figures 4L–S). In particular, the intramolecular N-terminal RFP showed 84.8% (\pm 4.6% SD) colocalization while the C-terminally located RFP showed 44.4% (\pm 2.4% SD) colocalization (Figure 4T). Thus, both the dually tagged and the single tagged constructs reveal a closer apposition of the N-terminal region of Bassoon with TGN38 than its C-terminal region. In addition, single tagged Bsn-mRFP did not colocalize with CFP-Golgi (Supplementary Figure 3). This indicates that, while the *c*-terminal is located farther away from TGN38 than the intramolecular tag, it does not colocalize with the *trans*-Golgi compartment.

Next, we quantified the distribution pattern of tagged Bassoon termini at certain distances relative to the TGN. To this end, we defined two distance categories, i.e., 0–100 nm and 101 nm–1 μ m from TGN38 signals. We excluded Bassoon signals farther than 1 μ m from TGN38 signals, assuming that these signals were not associated with the TGN. The intramolecular N-terminal tags of both double- and single-tagged Bassoon predominantly occupied the 0–100-nm-distance range. Fraction sizes were 0.67 ± 0.1 SD for RFP-Bsn-GFP and 0.84 ± 0.04 SD for RFP-Bsn. A smaller fraction of each construct occupied the 101-nm–1- μ m distance range. Here, fraction sizes were 0.33 ± 0.1 SD for RFP-Bsn-GFP and 0.15 ± 0.04 SD RFP-Bsn (Figure 4U). In contrast to the intramolecular N-terminal tags, the C-terminal tags of all constructs were more evenly distributed between the two categories, with a tendency toward localization in the 101- to 1- μ m range: a slightly larger fraction of RFP-Bsn-GFP (0.63 ± 0.1 SD) and Bsn-RFP (0.55 ± 0.03 SD) resided within 101 nm–1 μ m, and the remaining smaller fraction of signals for double- (0.37 ± 0.1 SD) and single-tagged (0.45 ± 0.03 SD) Bassoon constructs was present within the 0–100-nm distance range (Figure 4U). Thus, all constructs were distributed in such a way that the intramolecular N-terminal tag had a greater likelihood for detection within 100 nm of TGN38 than the C-terminal tag. Overall, both the percentage of colocalization and the distance distribution indicate an orientation of recombinant Bassoon at the TGN where the N-termini are arranged closer to the TGN than their C-termini.

Is this arrangement of Bassoon specific for the localization of Bassoon relative to one particular Golgi-protein, i.e., TGN38? Or does it reflect the orientation of Bassoon relative to the TGN compartment in general? To assess this, we imaged RFP-Bsn, Bsn-RFP, and RFP-Bsn-EGFP in neurons immunostained for another TGN marker, i.e., Syntaxin6 (Syn6). As seen before with TGN38, the percentage of colocalization with Syn6 was higher for the intramolecular N-terminal tags of RFP-Bsn-EGFP (71.8%) and RFP-Bsn (75.8%) than for the C-terminal tags of RFP-Bsn-EGFP (23.8%) and Bsn-RFP (43.7%; Figures 5A–Q). The distance analysis also revealed a similar pattern compared with what was seen for TGN38: a significantly larger fraction of intramolecular N-terminal than C-terminal Bassoon signals of single- (0.8 ± 0.03 SD) and double-tagged (0.71 ± 0.02 SD) Bassoon constructs were distributed within the 0- to 100-nm distance range (Figure 5R).

Again, the C-terminal tags of both constructs were more evenly distributed between the two distance categories, and again, with a tendency toward localization in the 101- to 1- μ m range, i.e., a slight majority of C-terminal Bassoon signals of the single- (0.62 ± 0.03 SD) and double-tagged (0.65 ± 0.04 SD) constructs were present in the 101-nm to 1- μ m range from the nearest Syn6 signal (**Figure 5R**). These results show that Bassoon molecules possess similar colocalization and distance distribution relative to both Syn6 and TGN38 markers of the TGN. This suggests that Bassoon molecules are similarly oriented all over the TGN lamellae, with the N-terminus more closely associated with the TGN membrane than the C-terminus.

Which Domains of Bassoon Are Involved in Orienting the Molecule?

Next, we aimed at characterizing the features of Bassoon required for bringing the N-terminal region of Bassoon into close apposition to the TGN. N-myristoylation is an obvious possibility for anchoring a protein to membranes. Therefore, we generated a point-mutated version of the dually tagged Bassoon construct, called G2A-Bsn, where we replaced glycine in Position 2 with alanine. Dual-color STED images of TGN38 and the intramolecular N-terminal tag or the C-terminal tag of G2A-Bsn revealed the previously seen pattern of high colocalization of the intramolecular N-terminal tag (74.5%) and low colocalization (28.2%) of the C-terminal tag with TGN38 (**Figures 6A–H,Q**). Signals from the intramolecular N-terminal tag were predominantly (fraction size 0.75 ± 0.02 SD) located within 0–100 nm from the TGN38, while the majority of signals from the C-terminal tag (fraction size 0.75 ± 0.02 SD) were distributed within 101 nm–1 μ m from the TGN (**Figure 6R**). A functional N-myristoylation site is thus not necessary for the orientation of recombinant Bassoon at the TGN. These results do not exclude the possibility that the G2A-mutant recombinant Bassoon dimerizes with endogenous Bassoon, and that the intact endogenous Bassoon somehow helps orienting the N-terminus of the mutant protein. However, when we expressed G2A-Bsn in cultures obtained from mice lacking Bassoon, the intramolecular N-terminal tag of G2A-Bsn was still oriented toward the TGN, further corroborating that a functional N-myristoylation site is not necessary for the orientation of Bassoon at the TGN (**Supplementary Figure 4**).

Since an intact N-myristoylation consensus site was not required for the orientation of Bassoon, we wondered if any other sequences upstream of the intramolecular N-terminal tag were required for the orientation of Bassoon. To test this, we expressed the previously generated GFP-Bsn95-3938 construct, aka GFP-95-Bsn. In this construct, the N-terminal 94 amino acids are replaced by EGFP, but it accumulates at the Golgi-apparatus and at synapses (Dresbach et al., 2003, 2006). The EGFP tag of this construct, detected by our GFP-nanobody, displayed remarkably low colocalization with TGN38 at the nanoscopical level (**Figures 6I–L**). Its colocalization with TGN38 was 36.2% and the majority of these signals (0.60 ± 0.04 SD) were located farther than 100 nm from the nearest TGN38 signals (**Figures 6Q,R**), suggesting that sequences in the first

94 amino acids contribute to orienting the N-terminal area of Bassoon toward the TGN.

A central region of Bassoon, comprising amino acids 2,088–2,563 and termed Bsn-GBR (for Golgi-binding region), is required for targeting Bassoon to the Golgi-apparatus. Thus, this region may contribute to bringing parts of Bassoon into close proximity to the TGN. A construct consisting of these amino acids fused to the C-terminus of EGFP, indeed, targets the Golgi-apparatus, presumably *via* dimerization with endogenous Bassoon (Dresbach et al., 2006; Maas et al., 2012). Where is this construct located relative to TGN38 at the nanoscopical level? Our STED analysis revealed a relatively low colocalization with TGN38 (41.5%) and predominant signal allocations (0.67 ± 0.03 SD) in the 101-nm–1- μ m distance range from TGN38 signals (**Figures 6M–P,Q,R**). Thus, this region alone, while harboring Golgi-targeting capacity, cannot account for the close apposition of the N-terminal Bassoon regions to the TGN.

Together, these results indicate that neither of the two regions of Bassoon equipped with known Golgi-targeting sequences, i.e., the N-myristoylation consensus site and amino acids 2,088–2,563, account for the particular orientation of Bassoon at the TGN. Instead, the first 94 amino acids of Bassoon contribute to orienting the N-terminal region of Golgi-associated Bassoon toward the TGN.

Estimating the Extension of Bassoon Molecules at the *Trans*-Golgi Network

Having analyzed the distribution of N- and C-terminal tags over two distance categories, i.e., within 100 nm of TGN38 signals and between 101 nm and 1 μ m from the TGN, we wondered whether we might be able to extract the average distance between a tag and TGN38 from the data sets. **Figure 7A** shows the distances of signals relative to TGN38 obtained from all Bassoon constructs and tags, displayed as violin plots.

The analysis shows that most signals were located within 220 nm from the TGN, irrespective of the construct and the tag. Among these signals, two differences between the constructs were obvious: first, the median of the values for distance from TGN38 was smaller for the intramolecular N-terminal tags, both in the dually tagged construct and in the single-tagged construct, compared with all other constructs; second, wider sections of the violin plot, representing a higher probability that data in the population take on a certain value, indicated clustering of intramolecular N-terminal signals close to TGN38. In contrast, all other constructs showed a more uniform distribution of signals across the 0–220-nm range (**Figure 7A**). We then analyzed the signals from this 0–220 nm range to extract the average distances for each of the constructs and tags from TGN38 (**Figure 7B**). In dually tagged Bassoon, average distances from TGN38 were 69 nm for the intramolecular N-terminal tag and 115 nm for the C-terminal tag. Thus, amino acid 97 of Bassoon, where the intramolecular N-terminal tag is located, and amino acid 3938, where the C-terminal tag is located, are estimated to be 46 nm from each other. In single-tagged constructs, the intramolecular N-terminal tag was, on average, 48 nm away from TGN38; the C-terminal tag was 100 nm away. This yields an estimated

distance of 52 nm between the average location of the two tags. The average distances from TGN38 of GFP-Bsn95-3938 (106 nm) and Bsn-GBR (115 nm) show that the tags of these deletion constructs occupy similar locations compared with the C-terminal tags of full-length Bassoon constructs (**Figure 7B**).

In summary, both transfection of a dually tagged construct and separate transfections of single-tagged constructs lead to similar conclusions: first, the intramolecular N-terminal tag is located closer to TGN38 than the C-terminal tag; second, the average distance from TGN38 is between 48 and 69 nm for the intramolecular N-terminal tags; the average distance from TGN38 is between 100 and 115 nm for the C-terminal tags; third, the distance between the intramolecular N-terminal and the C-terminal tag is estimated to be between 46 and 52 nm. Overall, this indicates an orderly arrangement of Bassoon molecules with the N-terminus facing the TGN membrane (**Figure 7C**).

DISCUSSION

Bassoon is a presynaptic scaffold protein predicted to be up to 80 nm long (Gundelfinger et al., 2016). At active zones, Bassoon appears to have an extended conformation with its C-terminus facing the plasma membrane (Dani et al., 2010; Limbach et al., 2011). At synapses, Bassoon may thus represent one of the filamentous structures or dense projections characteristic of active zones (Dresbach et al., 2001; Phillips et al., 2001). Here, we find that recombinant Bassoon expressed in cultured hippocampal neurons has an extended conformation at the Golgi-apparatus. At this subcellular site, the N-terminus of Bassoon faces the TGN membrane. The fact that Bassoon is an extended protein already at this early stage of its trafficking path supports the notion that primordial active zone scaffolds assemble at the Golgi-apparatus (Dresbach et al., 2006). Its orientation relative to membranes, i.e., with the N-terminus facing the TGN membrane and the C-terminus facing the active zone plasma membrane – adds new insights and raises questions on the topology of its trafficking from the Golgi apparatus to active zones.

Design and Validation of the Constructs

To introduce a tag close to the N-terminus but outside the N-myristoylation consensus sequence, we placed mRFP or mGFP downstream of amino acid 97 in the new Bassoon constructs. Originally, this location was chosen because it contains a conveniently located HindIII-cloning site in rat Bassoon cDNA. Later, it became clear that the first 94 amino acids appear to be a structurally compact unit without persistent folding (Gundelfinger et al., 2016). Glycine and proline constitute 48% of the first 94 amino acids of rat Bassoon (25 glycine residues and 20 proline residues), while this percentage steeply drops to 18% in amino acids 95–197. Because of the location of the intramolecular tag, the new full-length constructs are expected to combine the properties of two previously characterized constructs: Amino acids 95–3,938 preceded by EGFP are correctly targeted to the Golgi-apparatus and to synapses (Dresbach et al., 2003, 2006;

Bresler et al., 2004; Tsuruel et al., 2009), and amino acids 1–97 followed by EGFP retain targeting capacity for the Golgi-apparatus through their N-myristoylation site (Dresbach et al., 2003, 2006). To avoid problems sometimes associated with co-expression, one of our new constructs is dually tagged, with an N-terminal intramolecular mRFP and C-terminal mGFP.

The use of recombinant protein bears the inherent caveat of overexpression. However, recombinant Bassoon has been used widely by us and others to monitor synapse assembly and turnover (Shapira et al., 2003; Cai et al., 2007; Lee et al., 2008; Tsuruel et al., 2009; Matz et al., 2010). In addition, our recombinant proteins accumulated at the expected subcellular sites, and the dually tagged construct showed the expected orientation at the synapse. The design of the constructs also provides several advantages. Under ideal expression conditions, the location of the N-terminal intramolecular tag (downstream of amino acid 94) and the C-terminal tag (downstream of amino acid 3,938) should report the maximal extension of Bassoon more accurately compared with the routinely used antibodies, whose epitopes are located between amino acids 756 and 1,001 and between amino acids 3,908 and 3,938 (e.g., Dani et al., 2010). Indeed, we observed a distance of 46–52 nm between the tags, compared with 30-nm distance calculated for the two epitopes in Dani et al. (2010). This is consistent with the tags being farther apart within recombinant Bassoon than the two epitopes are in endogenous Bassoon. We emphasize, however, that Dani et al. (2010) performed an extensive 3D analysis of a large number of synapses in brain sections, while we only performed a proof-of-principle analysis for our construct, analyzing a set of synapses that appeared to be visible as side views in our cultured neurons.

Using nanobodies to detect the tags provides an additional advantage: because of their small size and direct coupling to fluorophores, nanobodies bring the fluorescent dye closer to the epitope compared with indirect immunofluorescence, using primary and secondary antibodies. The subclusters of recombinant Bassoon we detected with nanobodies are consistent with this increased spatial resolution. Maybe these nanobodies detect Bassoon arranged in the presynaptic particle web (Phillips et al., 2001). Overall, we conclude that our analysis of recombinant Bassoon at synapses yields results consistent with previous observations and shows that our approach provides at least similar spatial resolution as previous nanoscopical approaches. Based on these assumptions, we conducted our detailed analysis of recombinant Bassoon at the Golgi-apparatus.

Trans Golgi Versus Trans-Golgi Network

Stimulated emission depletion microscopy revealed that recombinant Bassoon colocalizes with two TGN markers, i.e., TGN38 and Syntaxin-6, but not with a TG sub-compartment marker (**Figures 1, 2** and **Supplementary Figure 3**). This supports and extends previous data showing that both endogenous and recombinant Bassoon colocalize with TGN38 and Syntaxin 6 upon confocal analysis (Dresbach et al., 2006; Maas et al., 2012). This further corroborates that the recombinant protein faithfully represents the localization of endogenous Bassoon. In addition, it narrows down the exact localization of recombinant Bassoon by showing that it is more closely

associated with the TGN than with the sub-compartment. This observation is particularly insightful because the recombinant sub-compartment marker we have used here was shown by electron microscopy to selectively label the most “trans” located lamellae of the Golgi stack, i.e., the one immediately preceding the TGN (Wittenmayer, 2014).

Localization and Orientation of Full-Length Bassoon at the *Trans*-Golgi Network

A key finding of our study is that the N-terminal, intramolecular tag of Bassoon was located closer to the TGN than the C-terminal tag. This was true both for the dually tagged Bassoon and for the two constructs that carried single mRFP tags. In addition, it was true both when we used TGN38 and when we used Syntaxin-6 as TGN markers. Finally, both colocalization analysis and the distance distribution of the Bassoon constructs indicated this. Thus, recombinant Bassoon is an extended protein located at the TGN, with the N-terminal area closer to the TGN than the C-terminus, and the majority of Bassoon molecules have this orientation.

The distance distribution also revealed that the N-terminal, intramolecular tag had a higher likelihood of being located within 100-nm from the TGN than being located inside the 100-nm–1- μ m range, whereas the C-terminal tag appeared to be distributed more evenly between the two distance regimes. On average, the two tags were located 46 nm away from each other in the dually tagged construct, and 52 nm away from each other when the two single tag constructs were compared. A distance of approximately 50 nm between the intramolecular tag and the C-terminal tag is well within the range of the 80-nm maximal extension of Bassoon predicted by Gundelfinger et al. (2016). It is also consistent with the two tags being farther apart within the primary structure of Bassoon than the two antibody epitopes used in Dani et al. (2010), who estimated a distance of 30 nm between those epitopes based on STORM data. Taken together, our data indicate that recombinant Bassoon is an extended protein located at the TGN, with its N-terminal area oriented toward the TGN membrane and the C-terminus farther away. In addition, they suggest an average distance of 46–52 nm between the intramolecular tag located downstream of amino acid 97 and the C-terminal tag located downstream of amino acid 3,938 of rat Bassoon.

Localization and Orientation of Deletion Constructs

Bassoon includes at least two regions with binding capacity for the Golgi-apparatus, including the myristoylated N-terminus and the region-spanning amino acids 2,088–2,563 called the Golgi-binding region (GBR). Using conventional epifluorescence microscopy, we had previously detected constructs encoding either one of these regions at the TGN (Dresbach et al., 2003, 2006). The results obtained from analyzing mutated constructs of Bassoon provided some novel insights and raised new questions.

First, the myristoylation-deficient G2A point mutant was still oriented with its N-terminus toward the TGN, even in Bassoon knockout cultures. Thus, insertion of myristic acid into the lipid

bilayer is not required for the orientation of the N-terminal region of Bassoon toward the TGN. Through its second coiled-coil domain, the G2A-mutant full-length protein may still bind to endogenous Piccolo (Maas et al., 2012). But it is unlikely that this helps orienting the N-terminus of Bassoon toward the TGN, because another construct, GFP-Bsn95-3938, which is also predicted to bind to endogenous Bassoon and Piccolo, showed an aberrant orientation. Thus, N-myristoylation appears to be dispensable for the orientation of Bassoon.

Second, as mentioned above, GFP-Bsn95-3938 was less closely associated with the TGN than the intramolecular tag in the full-length Bassoon constructs. This shows that the N-terminal 97 amino acids of Bassoon are essential for orienting the N-terminus of Bassoon toward the TGN. It is likely that the unusually high percentage of glycine and proline characteristic of this region of Bassoon contributes to this, but the mechanisms and putative binding partners providing this orientation have yet to be discovered. Surprisingly, the tag in GFP-Bsn95-3938 was located unexpectedly far away from the TGN and was rather distributed like the C-terminal tag of the full-length construct. We do not know if some extensive bending of the N-terminal end of this construct toward its C-terminus or a completely aberrant localization account for this.

Third, Bsn-GBR showed a similar localization. This construct includes the second coiled-coil domain of Bassoon, located between amino acids 2,246 and 2,366 of rat Bassoon (tom Dieck et al., 1998). Bsn-GBR harbors binding capacity for an unknown target site on the Golgi-apparatus and in addition, dimerizes or oligomerizes with endogenous Bassoon through the CC2 domain (Dresbach et al., 2006; Maas et al., 2012). Therefore, we expected that this construct might bind to the TGN or to a central region of endogenous Bassoon or both. In particular, we aimed to find out if Bsn-GBR locates to the same TGN site that the N-terminus of Bassoon locates to. However, this construct was located farther away from the TGN than the intramolecular tag of Bassoon and had a similarly widespread distribution like the C-terminal tag of full-length Bassoon.

What may account for this localization? Bassoon and Piccolo are required for the biogenesis of Golgi-derived transport vesicles, called gPTVs, that also contain the scaffold protein ELKS2 (Maas et al., 2012). Bassoon binds to ELKS2 through its CC3 regions, to the Golgi apparatus through at least two regions, and to CTBP1, a protein involved in the fission of vesicles budding from the Golgi-apparatus. Thus, Bassoon is endowed with binding capacity for proteins that, together, could, theoretically, mediate the generation and fission of gPTVs. Overexpressing Bsn-GBR causes the accumulation of Bassoon, Piccolo, and ELKS2 at the Golgi-apparatus. Bsn-GBR prevents forward trafficking of gPTVs either by preventing binding of endogenous Bassoon to the Golgi-apparatus, or by impairing oligomerization of Bassoon and possibly, Piccolo (Maas et al., 2012). Hence, a complex situation may arise where endogenous proteins gPTVs accumulate and where, in addition, endogenous proteins may be misplaced, when Bsn-GBR is overexpressed. Therefore, the relatively widespread distribution of Bsn-GBR at the nanoscopical level may reflect this construct binding to its target sites in a condition of reduced gPTV exit from the Golgi.

Overall, our results show that, at the nanoscopeical level, the Bsn-GBR does not bind to the same TGN-region as the N-terminus of Bassoon. Thus, the two Golgi-binding regions of Bassoon seem to associate with distinct sites at the Golgi-apparatus, and the N-terminal 95 amino acids fulfill a special role in orienting the N-terminus toward the TGN.

Perspective: Toward a Topological Scenario

At active zones, the C-terminus of Bassoon is located closer to the plasma membrane than the N-terminus (Dani et al., 2010; our study). Assuming that Bassoon travels to active zones on Golgi-derived Piccolo-Bassoon transport vesicles (gPTVs; Zhai et al., 2001; Maas et al., 2012), one might predict that the C-terminus of Bassoon is attached to Golgi-membranes and subsequently, to the gPTV membrane; deposition of Bassoon at synapses, perhaps by exocytotic fusion of the transport vesicle with the presynaptic plasma membrane, would then directly place the C-terminus close to the active zone membrane. This scenario is “simple” because it involves no topological rearrangements, i.e., the C-terminus of Bassoon is attached to equivalent membranes all along the trafficking route.

Here, we find that the N-terminus of Bassoon is oriented toward the TGN membrane, while the C-terminus is located farther away from it. In the context of the gPTV model (Zhai et al., 2001; Maas et al., 2012), this is consistent with the following scenario, which also involves no topological rearrangements: at the Golgi-apparatus, the N-terminus of Bassoon may be attached to TGN-associated synaptic vesicle precursor membranes, while the C-terminus may become attached – simultaneously or later – to gPTVs. In this way, Bassoon would travel out of the soma on gPTVs and, at the same time, carry along synaptic vesicle precursors *via* its N-terminal region. This speculative scenario is consistent with several observations. First, Bassoon constructs lacking N-terminal areas appear at synapses as small spots, the size of Piccolo immunosignals, suggesting that these constructs incorporate into the active zone cytomatrix immediately adjacent to the plasma membrane; in contrast, a construct comprised of the N-terminal 609 amino acids of Bassoon appears at synapses as larger spots similar to the size of entire synaptic vesicle clusters, suggesting that this N-terminal region of Bassoon may bind to synaptic vesicles (Dresbach et al., 2003). Second, clouds of clear-core vesicles, dense-core vesicles, and Bassoon were detected by electron immune-electron microscopy in axons (Tao-Cheng, 2007). It is possible that the dense core vesicles may represent gPTVs, while the clear-core vesicles represent synaptic vesicle precursors. Third, a substantial fraction of synaptic vesicles precursors, labeled by recombinant synaptophysin and called synaptic vesicle transport vesicles (STVs) in this study, co-traffics with active zone precursors, labeled by recombinant Bassoon, as revealed by live imaging studies (Bury and Sabo, 2011, 2016). Recently, a type of Golgi-derived precursor vesicle called PLV, for presynaptic lysosome-related vesicles, has been identified. PLVs are required for the transport of presynaptic material. They carry, in addition to lysosomal proteins, the synaptic vesicle protein VGlut1 and co-traffic with Bassoon (Vukoja et al., 2018). Thus,

at the Golgi-apparatus, Bassoon could connect to PTVs *via* its C-terminus and to synaptic vesicle precursors *via* its N-terminus, and in this way, generate already at the Golgi-apparatus, a topological scenario that is later encountered at active zones. Whether this scenario holds true will need to be investigated in future studies.

DATA AVAILABILITY STATEMENT

The original contributions presented in the study are included in the article/**Supplementary Material**, further inquiries can be directed to the corresponding author.

AUTHOR CONTRIBUTIONS

TG and TD: conceptualization and writing – original draft. TG: investigation. CM-V and AF: resources. TG, CM-V, AF, and TD: review manuscript. TD: funding acquisition and supervision. All authors contributed to the article and approved the submitted version.

FUNDING

This work was supported by the DFG Research Center for Nanoscale Microscopy and Molecular Physiology of the Brain (CNMPB) to TD.

ACKNOWLEDGMENTS

We are thankful to Stefan W. Hell, Dirk Kamin, and Fabian Göttfert for the training and guidance on the STED setups a Max Planck Institute of Biophysical Chemistry. We thank Irmgard Weiss for technical assistance.

SUPPLEMENTARY MATERIAL

The Supplementary Material for this article can be found online at: <https://www.frontiersin.org/articles/10.3389/fnmol.2021.744034/full#supplementary-material>

Supplementary Figure 1 | (A) Schematic of new Bassoon full-length constructs. Numbers indicate amino acid positions of rat Bassoon. GP indicates the glycine- and proline-rich region comprised of amino acids 1–97; Zn1 and Zn2 indicate zinc finger domains; cc1, cc2, and cc3 are coiled-coil domains; cc2 contains a Golgi-binding region (GBR) of Bassoon; QQ indicates the location of glutamine repeats. The regions-containing epitopes for commercially available antibodies used or discussed in our study are indicated as “mAB” for monoclonal antibody and “pAB” for polyclonal antibody. Green ovals represent mGFP, red ovals represent mRFP. **(B)** Amino acid sequences of regions containing tags in the novel constructs. Red font: mRFP; green font: mGFP; gray font: spacers; black font: rat Bassoon sequences. The c-terminal tags (either mRFP or mGFP) were placed downstream of the sequence WTRGPSI, where W (bold font) is amino acid 3938 of rat Bassoon. The intramolecular tags (either mRFP or mGFP) were placed downstream of serine 97 of rat Bassoon. The constructs were designed in such a way that Q95, A96, and S97 (QAS, indicated in bold font and underlined) were repeated downstream of the tags. G2, which is part of a predicted

N-myristoylation consensus site, is highlighted in blue. Glycine and proline residues located within the first 97 amino acids of Bassoon are highlighted in yellow to indicate their frequent occurrence in this region.

Supplementary Figure 2 | Full-length RFP-tagged Bassoon constructs localize at the TGN in young neurons, traffick to synaptic sites, and are incorporated into the insoluble AZ scaffold of mature neurons. Panel (A) is a schematic diagram of full-length Bassoon sequence compared with the sequence of mRFP-tagged Bassoon constructs, where M stands for N-myristoylation sequence, Zn1 and Zn2 are the two zinc finger domains, and cc1, cc2, and cc3 are the three predicted coiled-coil regions. Immunostained DIV5-7 (B-E, F-I) and DIV14 (J-P, Q-W) hippocampal neurons transfected with RFP-tagged Bassoon constructs, post a DIV3 lipofectamine transfection, are co-stained with the TGN38 (B-H), synaptophysin (J-L, Q-S), and piccolo (M-O, T-V). Panels (I, P) represent 40× over views of the transfections, and a and b represent the zooms of their white square ROIs, respectively. Neurons were fixed in cold methanol prior to PFA fixation to quench the RFP autofluorescence. $N = 10$ transfected neurons/condition imaged (B-I). (X) Is the Bassoon colocalization quantification for panels (J-W); data are represented as mean \pm SEM, $N = 32$ (RFP-BSN-Piccolo), 13 (BSN-RFP-Piccolo), 34 (RFP-BSN-Synaptophysin), 14 (BSN-RFP-Synaptophysin), images analyzed. $N = 2-3$ separate transfected neuronal cultures/independent experiments (B-W). Scale bars 10 μm (B, F, Q, J), 5 μm (C-G), and 2 μm (K-P, R-W).

Supplementary Figure 3 | Full-length C-terminally tagged Bassoon does not localize to the *trans*-Golgi sub-compartment labeled by CFP-Golgi. DIV7 hippocampal neurons were transfected with CFP-Golgi (a *trans*-Golgi sub-compartment marker) and full-length single-tagged Bsn- mRFP construct, and immunostained using GFP and/or RFP nanobodies against tagged constructs and from (A-E). Two-color STED images of Golgi sub-compartment marker CFP-Golgi

and RFP-Bsn constructs (C-E). (A) shows wide field overview of transfected constructs, (B) the confocal zooms of the soma, inset a reflects the single channels and merged full STED deconvolved (Deconv.) images of (C-E), while inset b represents the zooms of STED images. $N = 10$ images of transfected neuronal somas imaged as technical replicates $N = 2$ separate neuronal cultures/independent experiments. Scale bars 4 μm (B) and 1 μm (E).

Supplementary Figure 4 | Orientation of G2A-mRFP-Bsn-mEGFP myristoyl mutant construct in endogenous Bassoon-free *Bsn*^{-/-} knockout mice and their *Bsn*^{+/+} wild-type littermates. DIV7 *Bsn*^{+/+} (A-H) and *Bsn*^{-/-} (I-M) sandwich hippocampal cultures were transfected with G2A-mRFP-Bsn-mEGFP. Two-color STED images with their respective insets are shown for the N- (A-D, I-L) and C- (E-H, M-P) termini of the myristoyl mutant construct, respectively. Immunostaining was performed using RFP-nanobody-Atto594 or GFP-nanobody-Atto647 and a TGN38 marker. Graphs (Q, R) were represented as mean \pm SD, $N = 4$ transfected neuronal soma image/condition. Data are represented as mean \pm SEM. $N = 2$ knockout and two wild-type animals. Quantified and statistically tested with a Tukey's multiple comparisons test for amount of colocalization and signal distributions, respectively, * $p \leq 0.05$, ** $p \leq 0.01$, and *** $p \leq 0.001$. Scale bars 1 μm (A-P).

Supplementary Figure 5 | Raw and deconvolved images of Figure 4 and Figure 5 transfected full-length Bassoon constructs. Transfections were performed in DIV7 hippocampal cultured neurons. The Bassoon signals are visualized by GFP/RFP nanobodies and co-stained with the TGN38/Syn6 marker. Raw STED data with individual channels and merged overviews of each image and the following row show the same images after Richardson Lucy deconvolution. $N = 10$ transfected neurons/condition imaged and $N = 2$ separate transfected neuronal cultures/independent experiments. Scale Bar = 1 μm .

REFERENCES

- Acuna, C., Liu, X., and Südhof, T. C. (2016). How to Make an Active Zone: unexpected Universal Redundancy between RIMs and RIM-BPs. *Neuron* 91, 792–807. doi: 10.1016/j.neuron.2016.07.042
- Bresler, T., Shapira, M., Boeckers, T., Dresbach, T., Futter, M., Garner, C. C., et al. (2004). Postsynaptic density assembly is fundamentally different from presynaptic active zone assembly. *J. Neurosci.* 24, 1507–1520. doi: 10.1523/JNEUROSCI.3819-03.2004
- Bury, L. A. D., and Sabo, S. L. (2011). Coordinated trafficking of synaptic vesicle and active zone proteins prior to synapse formation. *Neural Dev.* 6:24. doi: 10.1186/1749-8104-6-24
- Bury, L. A. D., and Sabo, S. L. (2016). Building a Terminal: mechanisms of Presynaptic Development in the CNS. *Neuroscientist* 22, 372–391. doi: 10.1177/1073858415596131
- Cai, Q., Pan, P.-Y., and Sheng, Z.-H. (2007). Syntabulin-kinesin-1 family member 5B-mediated axonal transport contributes to activity-dependent presynaptic assembly. *J. Neurosci.* 27, 7284–7296. doi: 10.1523/JNEUROSCI.0731-07.2007
- Cases-Langhoff, C., Voss, B., Garner, A. M., Appeltauer, U., Takei, K., Kindler, S., et al. (1996). Piccolo, a novel 420 kDa protein associated with the presynaptic cytomatrix. *Eur. J. Cell Biol.* 69, 214–223.
- Dani, A., Huang, B., Bergan, J., Dulac, C., and Zhuang, X. (2010). Superresolution imaging of chemical synapses in the brain. *Neuron* 68, 843–856. doi: 10.1016/j.neuron.2010.11.021
- Davydova, D., Marini, C., King, C., Klueva, J., Bischof, F., Romorini, S., et al. (2014). Bassoon specifically controls presynaptic P/Q-type Ca(2+) channels via RIM-binding protein. *Neuron* 82, 181–194. doi: 10.1016/j.neuron.2014.02.012
- Dresbach, T., Hempelmann, A., Spilker, C., tom Dieck, S., Altmann, W. D., Zuschratter, W., et al. (2003). Functional regions of the presynaptic cytomatrix protein bassoon: significance for synaptic targeting and cytomatrix anchoring. *Mol. Cell. Neurosci.* 23, 279–291. doi: 10.1016/S1044-7431(03)00015-0
- Dresbach, T., Qualmann, B., Kessels, M. M., Garner, C. C., and Gundelfinger, E. D. (2001). The presynaptic cytomatrix of brain synapses. *Cell. Mol. Life Sci.* 58, 94–116. doi: 10.1007/PL00000781
- Dresbach, T., Torres, V., Wittenmayer, N., Altmann, W. D., Zamorano, P., Zuschratter, W., et al. (2006). Assembly of active zone precursor vesicles: obligatory trafficking of presynaptic cytomatrix proteins Bassoon and Piccolo via a *trans*-Golgi compartment. *J. Biol. Chem.* 281, 6038–6047. doi: 10.1074/jbc.M508784200
- Fenster, S. D., Chung, W. J., Zhai, R., Cases-Langhoff, C., Voss, B., Garner, A. M., et al. (2000). Piccolo, a presynaptic zinc finger protein structurally related to bassoon. *Neuron* 25, 203–214. doi: 10.1016/S0896-6273(00)80883-1
- Garner, C. C., Kindler, S., and Gundelfinger, E. D. (2000). Molecular determinants of presynaptic active zones. *Curr. Opin. Neurobiol.* 10, 321–327. doi: 10.1016/S0959-4388(00)00093-3
- Good, M. C., Zalatan, J. G., and Lim, W. A. (2011). Scaffold proteins: hubs for controlling the flow of cellular information. *Science* 332, 680–686. doi: 10.1126/science.1198701
- Griffiths, G., and Simons, K. (1986). The *trans* golgi network: sorting at the exit site of the golgi complex. *Science* 234, 438–443. doi: 10.1126/science.2945253
- Gundelfinger, E. D., Reissner, C., and Garner, C. C. (2016). Role of Bassoon and Piccolo in Assembly and Molecular Organization of the Active Zone. *Front. Synaptic Neurosci.* 7:19. doi: 10.3389/fnsyn.2015.00019
- Hallermann, S., Fejtova, A., Schmidt, H., Weyhersmüller, A., Silver, R. A., Gundelfinger, E. D., et al. (2010). Bassoon speeds vesicle reloading at a central excitatory synapse. *Neuron* 68, 710–723. doi: 10.1016/j.neuron.2010.10.026
- Hamers-Casterman, C., Atarhouch, T., Muyldermans, S., Robinson, G., Hamers, C., Songa, E. B., et al. (1993). Naturally occurring antibodies devoid of light chains. *Nature* 363, 446–448. doi: 10.1038/363446a0
- Harris, L. J., Skaletsky, E., and McPherson, A. (1998). Crystallographic structure of an intact IgG1 monoclonal antibody. *J. Mol. Biol.* 275, 861–872. doi: 10.1006/jmbi.1997.1508
- Held, R. G., Liu, C., Ma, K., Ramsey, A. M., Tarr, T. B., De Nola, G., et al. (2020). Synapse and Active Zone Assembly in the Absence of Presynaptic Ca2+ Channels and Ca2+ Entry. *Neuron* 107, 667–683.e9. doi: 10.1016/j.neuron.2020.05.032
- Hoffmann-Conaway, S., Brockmann, M. M., Schneider, K., Annamneedi, A., Rahman, K. A., Bruns, C., et al. (2020). Parkin contributes to synaptic vesicle autophagy in Bassoon-deficient mice. *Elife* 9:e56590. doi: 10.7554/eLife.56590.sa2
- Imig, C., Min, S.-W., Krinner, S., Arancillo, M., Rosenmund, C., Südhof, T. C., et al. (2014). The morphological and molecular nature of synaptic vesicle priming at

- presynaptic active zones. *Neuron* 84, 416–431. doi: 10.1016/j.neuron.2014.10.009
- Lee, S.-H., Peng, I.-F., Ng, Y. G., Yanagisawa, M., Bamji, S. X., Elia, L. P., et al. (2008). Synapses are regulated by the cytoplasmic tyrosine kinase Fer in a pathway mediated by p120catenin, Fer, SHP-2, and beta-catenin. *J. Cell Biol.* 183, 893–908. doi: 10.1083/jcb.200807188
- Limbach, C., Laue, M. M., Wang, X., Hu, B., Thiede, N., Hultqvist, G., et al. (2011). Molecular in situ topology of Aczonin/Piccolo and associated proteins at the mammalian neurotransmitter release site. *Proc. Natl. Acad. Sci. U. S. A.* 108, E392–E401. doi: 10.1073/pnas.1101707108
- Maas, C., Torres, V. I., Altmann, W. D., Leal-Ortiz, S., Wagh, D., Terry-Lorenzo, R. T., et al. (2012). Formation of Golgi-derived active zone precursor vesicles. *J. Neurosci.* 32, 11095–11108. doi: 10.1523/JNEUROSCI.0195-12.2012
- Matz, J., Gilyan, A., Kolar, A., McCarvill, T., and Krueger, S. R. (2010). Rapid structural alterations of the active zone lead to sustained changes in neurotransmitter release. *Proc. Natl. Acad. Sci. U. S. A.* 107, 8836–8841. doi: 10.1073/pnas.0906087107
- Mellman, I., and Simons, K. (1992). The golgi complex: in vitro veritas. *Cell* 68, 829–840. doi: 10.1016/0092-8674(92)90027-A
- Mendoza Schulz, A., Jing, Z., Sánchez Caro, J. M., Wetzel, F., Dresbach, T., Strenzke, N., et al. (2014). Bassoon-disruption slows vesicle replenishment and induces homeostatic plasticity at a CNS synapse. *EMBO J.* 33, 512–527. doi: 10.1002/emboj.201385887
- Montenegro-Venegas, C., Fienko, S., Anni, D., Pina-Fernandez, E., Frischknecht, R., and Fejtova, A. (2021). Bassoon inhibits proteasome activity via interaction with PSMB4. *Cell. Mol. Life Sci.* 78, 1545–1563. doi: 10.1007/s00018-020-03590-z
- Okerlund, N. D., Schneider, K., Leal-Ortiz, S., Montenegro-Venegas, C., Kim, S. A., Garner, L. C., et al. (2017). Bassoon Controls Presynaptic Autophagy through Atg5. *Neuron* 93, 897–913.e7. doi: 10.1016/j.neuron.2017.01.026
- Phillips, G. R., Huang, J. K., Wang, Y., Tanaka, H., Shapiro, L., Zhang, W., et al. (2001). The presynaptic particle web: ultrastructure, composition, dissolution, and reconstitution. *Neuron* 32, 63–77. doi: 10.1016/S0896-6273(01)00450-0
- Ries, J., Kaplan, C., Platonova, E., Eghlidi, H., and Ewers, H. (2012). A simple, versatile method for GFP-based super-resolution microscopy via nanobodies. *Nat. Methods* 9, 582–584. doi: 10.1038/nmeth.1991
- Shapira, M., Zhai, R. G., Dresbach, T., Bresler, T., Torres, V. I., Gundelfinger, E. D., et al. (2003). Unitary assembly of presynaptic active zones from Piccolo-Bassoon transport vesicles. *Neuron* 38, 237–252. doi: 10.1016/S0896-6273(03)00207-1
- Südhof, T. C. (2012). The presynaptic active zone. *Neuron* 75, 11–25. doi: 10.1016/j.neuron.2012.06.012
- Tao-Cheng, J.-H. (2007). Ultrastructural localization of active zone and synaptic vesicle proteins in a preassembled multi-vesicle transport aggregate. *Neuroscience* 150, 575–584. doi: 10.1016/j.neuroscience.2007.09.031
- tom Dieck, S., Sanmartí-Vila, L., Langnaese, K., Richter, K., Kindler, S., Soyke, A., et al. (1998). Bassoon, a novel zinc-finger CAG/glutamine-repeat protein selectively localized at the active zone of presynaptic nerve terminals. *J. Cell Biol.* 142, 499–509. doi: 10.1083/jcb.142.2.499
- Tsuriel, S., Fisher, A., Wittenmayer, N., Dresbach, T., Garner, C. C., and Ziv, N. E. (2009). Exchange and redistribution dynamics of the cytoskeleton of the active zone molecule bassoon. *J. Neurosci.* 29, 351–358. doi: 10.1523/JNEUROSCI.4777-08.2009
- Tsuriel, S., Geva, R., Zamorano, P., Dresbach, T., Boeckers, T., Gundelfinger, E. D., et al. (2006). Local sharing as a predominant determinant of synaptic matrix molecular dynamics. *PLoS Biol.* 4:e271. doi: 10.1371/journal.pbio.0040271
- Vukoja, A., Rey, U., Petzoldt, A. G., Ott, C., Vollweiler, D., Quentin, C., et al. (2018). Presynaptic Biogenesis Requires Axonal Transport of Lysosome-Related Vesicles. *Neuron* 99, 1216–1232.e7. doi: 10.1016/j.neuron.2018.08.004
- Waites, C. L., Leal-Ortiz, S. A., Okerlund, N., Dalke, H., Fejtova, A., Altmann, W. D., et al. (2013). Bassoon and Piccolo maintain synapse integrity by regulating protein ubiquitination and degradation. *EMBO J.* 32, 954–969. doi: 10.1038/emboj.2013.27
- Wang, X., Kibschull, M., Laue, M. M., Lichte, B., Petrasch-Parwez, E., and Kilimann, M. W. (1999). Aczonin, a 550-kD putative scaffolding protein of presynaptic active zones, shares homology regions with Rim and Bassoon and binds profilin. *J. Cell Biol.* 147, 151–162. doi: 10.1083/jcb.147.1.151
- Wildanger, D., Medda, R., Kastrop, L., and Hell, S. W. (2009b). A compact STED microscope providing 3D nanoscale resolution. *J. Microsc.* 236, 35–43. doi: 10.1111/j.1365-2818.2009.03188.x
- Wildanger, D., Bückers, J., Westphal, V., Hell, S. W., and Kastrop, L. (2009a). A STED microscope aligned by design. *Opt. Express* 17, 16100–16110. doi: 10.1364/OE.17.016100
- Wittenmayer, N. (2014). Photoconversion of CFP to study neuronal tissue with electron microscopy. *Methods Mol. Biol.* 1148, 77–87. doi: 10.1007/978-1-4939-0470-9_6
- Zhai, R. G., Vardinon-Friedman, H., Cases-Langhoff, C., Becker, B., Gundelfinger, E. D., Ziv, N. E., et al. (2001). Assembling the presynaptic active zone: a characterization of an active one precursor vesicle. *Neuron* 29, 131–143. doi: 10.1016/S0896-6273(01)00185-4

Conflict of Interest: The authors declare that the research was conducted in the absence of any commercial or financial relationships that could be construed as a potential conflict of interest.

Publisher's Note: All claims expressed in this article are solely those of the authors and do not necessarily represent those of their affiliated organizations, or those of the publisher, the editors and the reviewers. Any product that may be evaluated in this article, or claim that may be made by its manufacturer, is not guaranteed or endorsed by the publisher.

Copyright © 2021 Ghelani, Montenegro-Venegas, Fejtova and Dresbach. This is an open-access article distributed under the terms of the Creative Commons Attribution License (CC BY). The use, distribution or reproduction in other forums is permitted, provided the original author(s) and the copyright owner(s) are credited and that the original publication in this journal is cited, in accordance with accepted academic practice. No use, distribution or reproduction is permitted which does not comply with these terms.